



# Full-length cellular $\beta$ -secretase has a trimeric subunit stoichiometry, and its sulfur-rich transmembrane interaction site modulates cytosolic copper compartmentalization

Received for publication, January 31, 2017, and in revised form, June 9, 2017. Published, Papers in Press, June 21, 2017, DOI 10.1074/jbc.M117.779165

Filip Liebsch<sup>‡</sup>, Mark R. P. Arousseau<sup>§1</sup>, Tobias Bethge<sup>¶2</sup>, Hugo McGuire<sup>||3</sup>, Silvia Scolari<sup>\*\*</sup>, Andreas Herrmann<sup>\*\*</sup>, Rikard Blunck<sup>||4</sup>, Derek Bowie<sup>‡5</sup>, and Gerd Multhaup<sup>‡55</sup>

From the <sup>‡</sup>Integrated Program in Neuroscience, McGill University, Montreal, Quebec H3G 0B1, Canada, the <sup>§</sup>Department of Pharmacology & Therapeutics, McGill University, Montreal, Quebec H3G 1Y6, Canada, the <sup>¶</sup>Institut für Chemie und Biochemie, Freie Universität Berlin, 14195 Berlin, Germany, the <sup>||</sup>Department of Physics, Université de Montréal, Montreal, Quebec H3C 3J7, Canada, and the <sup>\*\*</sup>Institut für Biologie, Humboldt Universität zu Berlin, 10115 Berlin, Germany

Edited by Paul E. Fraser

The  $\beta$ -secretase (BACE1) initiates processing of the amyloid precursor protein (APP) into A $\beta$  peptides, which have been implicated as central players in the pathology of Alzheimer disease. BACE1 has been described as a copper-binding protein and its oligomeric state as being monomeric, dimeric, and/or multimeric, but the native cellular stoichiometry has remained elusive. Here, by using single-molecule fluorescence and *in vitro* cross-linking experiments with photo-activatable unnatural amino acids, we show that full-length BACE1, independently of its subcellular localization, exists as trimers in human cells. We found that trimerization requires the BACE1 transmembrane sequences (TMSs) and cytoplasmic domains, with residues Ala<sup>463</sup> and Cys<sup>466</sup> buried within the trimer interface of the sulfur-rich core of the TMSs. Our 3D model predicts that the sulfur-rich core of the trimeric BACE1 TMS is accessible to metal ions, but copper ions did not trigger trimerization. The results of functional assays of endogenous BACE1 suggest that it has a role in intracellular copper compartmentalization by transferring cytosolic copper to intracellular compartments, while leaving the overall cellular copper concentration unaltered. Adding to existing physiological models, our results provide novel insight into the atypical interactions between copper and BACE1 and into its non-enzymatic activities. In conclusion, therapeutic Alzheimer disease prevention strategies aimed at decreasing BACE1 protein levels should be regarded with caution, because adverse effects in copper homeostasis may occur.

This work was supported in part by Natural Sciences and Engineering Research Council of Canada (NSERC) Grant RGPIN 04774-15, the Canada Foundation for Innovation (CFI), Canada Research Chairs (CRC) Program, and the International Copper Association (to G. M.), Studienstiftung des Deutschen Volkes and Groupe de Recherche Axé sur la Structure des Protéines (GRASP) Ph.D. fellowships (to F.L.), operating grants from the Canadian Institutes of Health Research (CIHR) (to D. B.), and the Fonds de recherche du Québec, Santé (FRQS). The authors declare that they have no conflicts of interest with the contents of this article.

This article contains supplemental Figs. S1–S7.

<sup>1</sup> Supported by a Banting and Best graduate fellowship from the CIHR.

<sup>2</sup> Present address: Institute for Laboratory Medicine, Kantonsspital Aarau, CH-5001 Aarau, Switzerland.

<sup>3</sup> Supported by a Fonds de recherche du Québec – Nature et technologies (FRQNT) doctoral research grant.

<sup>4</sup> Supported by NSERC Grant DG 327201-2012 and CIHR Grant MOP 136894.

<sup>5</sup> To whom correspondence should be addressed. Tel.: 514-398-3621; Fax: 514-398-2045; E-mail: gerhard.multhaup@mcgill.ca.

The  $\beta$ -secretase (BACE1)<sup>6</sup> was first identified as the shed-dase that cleaves the amyloid precursor protein (APP) in the amyloidogenic pathway that leads to amyloid- $\beta$  (A $\beta$ ) formation, which is ultimately linked to the pathology of Alzheimer disease (1, 2). BACE1 is unique among aspartic acid proteases through its single transmembrane sequence (TMS) that links the ectodomain to a short cytosolic C-terminal tail (2).

BACE1 cleaves APP into the soluble sAPP $\beta$  and alternative membrane-bound  $\beta$ -C-terminal fragments,  $\beta$ - and  $\beta'$ -CTF (3). In subsequent processing steps by the  $\gamma$ -secretase complex, A $\beta$  species of varying lengths are generated (4). The BACE1 TMS is required to access cellular substrates such as APP (5). BACE1 lacking the TMS cleaves APP to a lesser extent at the  $\beta'$  (= C89)-site (6). The identification of TMS-binding partners has also revealed the potential of this domain to modulate BACE1 protease activity. For example, the mammalian divalent cation tolerance homolog (CutA) is a TMS ligand that can regulate BACE1-mediated cleavage of APP (7). Similarly, a nonpeptidic compound, TAK-070, decreased levels of soluble A $\beta$  through interaction with the BACE1 TMS (8).

The cytosolic domain of BACE1 interacts with CCS, the copper chaperone of Cu/Zn-superoxide dismutase SOD1 (9, 10). Furthermore, a single Cu(I) ion binds there with high affinity to the C-terminal conserved amino acid residues and one of the cysteine residues in the C-terminal juxtamembrane region contributes critically to the binding site (9). The proposed TMS of BACE1, encompassing amino acids 458–478, harbors a conserved sulfur-rich Met<sup>462</sup>-XXX-Cys<sup>466</sup>-XXX-Met<sup>470</sup> motif with a Cu(I)-binding site that resembles the low-affinity copper-binding sites of the copper transport protein Ctr1 (11–14).

Despite past success in identifying the key physiological binding partners and substrates of BACE1 (15), relatively little is known about the assembly and functional stoichiometry of

<sup>6</sup> The abbreviations used are: BACE1,  $\beta$ -secretase 1; APP, amyloid precursor protein; CTF, C-terminal fragment; FLIM, fluorescence lifetime imaging; ANOVA, analysis of variance; TMS, transmembrane sequence(s); ROI, region(s) of interest; TIRF, total internal reflection fluorescence; GPI, glycosylphosphatidylinositol; BCS, bathocuproine disulfonate; pAzF, *p*-azido-L-phenylalanine; MRE, metal-responsive element; ICP-MS, inductively coupled plasma mass spectrometry; Tricine, *N*-[2-hydroxy-1,1-bis(hydroxymethyl)ethyl]glycine; BisTris, 2-[bis(2-hydroxyethyl)amino]-2-(hydroxymethyl)propane-1,3-diol; AU, absorbance unit.

BACE1 and its potential role as a metalloprotein in the cellular context. Metal ions can have structural roles, ~30% of all folded proteins bind metal ions (16), and some enzymes require metal ions as cofactors (17). For example, copper trafficking within a cell is strictly regulated and copper homeostasis is a highly sophisticated process conducted by soluble and membrane proteins to regulate uptake, distribution, and export of copper (18). Human disorders due to genetic predispositions cause disturbances of copper homeostasis, like copper deficiency or overload. Mutations in the copper transporting P-type ATPases Atp7a and Atp7b lead to Menkes (19) or Wilson diseases (20), respectively.

The present study advances our understanding of BACE1 as a copper-binding protein and the previously characterized Met<sup>462</sup>-XXX-Cys<sup>466</sup>-XXX-Met<sup>470</sup> motif (14). Using FLIM-FRET measurements, we demonstrate that full-length BACE1 oligomerizes in live cells. Single subunit counting, a single-molecule fluorescence technique, revealed that BACE1 exists as trimers in the plasma membrane of human cells. Complementary experiments, including the site-specific incorporation of a photoactivatable unnatural amino acid, demonstrate the existence of a trimerization interface at the level of the TMS. Although the significance of copper binding to BACE1 had remained uncertain, we find here that cytosolic copper levels are modulated by endogenous BACE1, whereas APP processing remains unaltered. Cys<sup>466</sup> is the critical TMS residue that accounts for the observed decrease in cytosolic copper concentrations. Together, we provide valuable insight into the conformation of BACE1 and reveal a novel moonlighting function of BACE1 in copper homeostasis.

## Results

### BACE1 forms homotrimers in mammalian cells

To investigate the BACE1 quaternary structure in the cellular context, we used the highly sensitive method of fluorescence lifetime imaging (FLIM)-Förster resonance energy transfer (FRET) and assessed BACE1 homointeractions in living cells. We created C-terminally tagged BACE1-cyan fluorescent protein (CFP) and -yellow fluorescent protein (YFP) constructs (Fig. 1*a*), which localized to the plasma membrane and intracellular compartments (endoplasmic reticulum/Golgi) upon transient expression in HEK293T cells (Fig. 1, *b* and *c*). Both of the CFP- and YFP-labeled BACE1 proteins retained their enzymatic activity, as indicated by the APP-cleavage product sAPP $\beta$  (supplemental Fig. S1*a*). To determine FRET efficiency, we measured the fluorescence lifetime of the donor BACE1-CFP in the absence (Fig. 1*b*) or presence (Fig. 1*c*) of the acceptor YFP. The average lifetime ( $\tau_{av}$ ) of the donor was calculated from a decay curve by plotting the number of photons-per-pixels associated with the plasma membrane and then fitting the curve with two-exponential terms (Fig. 1, *b* and *c*). The  $\tau_{av}$  for BACE1-CFP alone was  $2.45 \pm 0.01$  ns, which was significantly reduced to  $2.26 \pm 0.01$  ns in the presence of the acceptor BACE1-YFP (one-way ANOVA  $F(7,848) = 34.83$ ,  $p < 0.0001$ , Tukey's post hoc test,  $p < 0.001$ ). This result indicates close proximity between the two fluorophores (Fig. 1*d*) and implies the occurrence of BACE1 as natural oligomers in living cells. Given that

(i) the  $\tau_{av}$  of BACE1-CFP did not significantly change upon co-transfection with an unrelated type I transmembrane fusion protein influenza A virus hemagglutinin (HA)-YFP (Tukey's post hoc test,  $p > 0.05$ ) and (ii) the  $\tau_{av}$  significantly increased to  $2.34 \pm 0.01$  ns upon co-transfection of BACE1-CFP/-YFP with non-fluorescent BACE1 (Tukey's post hoc test,  $p < 0.001$ ) (Fig. 1*d*), we concluded that the observed shortening in the  $\tau_{av}$  between BACE1-CFP and -YFP originated from specific interactions between the two proteins. To determine whether BACE1 homointeractions are dependent on subcellular localization, we compared the  $\tau_{av}$  of BACE1-CFP and BACE1-CFP/YFP in various regions of interest (ROIs), encompassing the plasma membrane, perinuclear region, and intracellular space (Fig. 1*e*). Although  $\tau_{av}$  for BACE1-CFP and BACE1-CFP/-YFP was found to be decreased in the perinuclear and intracellular ROIs compared with either plasma membrane or whole cell measurements, FRET efficiencies were not significantly different (Fig. 1*f*). In light of these results, we concluded that BACE1 homointeractions are independent of the subcellular localization.

To further examine the precise stoichiometry of BACE1 in mammalian cells, we used single subunit counting (21–23). We created a BACE1 construct with an N-terminal monomeric superfolder GFP tag (msfGFP-BACE1) (21) (Fig. 2*a*). The msfGFP-BACE1 fusion protein was expressed in HEK293T cells and retained its enzymatic activity as indicated by the detection of sAPP $\beta$  (supplemental Fig. S2*a*). Using total internal reflection fluorescence (TIRF) microscopy, msfGFP-BACE1 was detected at the cell surface, and low-expressing cells exhibiting well separated fluorescent spots were selected for further analysis (Fig. 2*b*). The number of photobleaching steps for each individual spot, corresponding to the number of fluorescent subunits in one complex, was analyzed using the software package “progressive idealization and filtering” (sample trace Fig. 2*b*) (21). Using a fixed fluorescence probability ( $p_m = 53\%$  (21)) (see “Experimental procedures”), the resulting step frequency distribution for msfGFP-BACE1 was best fit (sum of squared errors (S.E.<sup>2</sup>), S.E.<sup>2</sup> = 7.51) with the sum (to account for co-localization (21)) of a 3rd and a 6th order binomial distribution ( $n = 2086$  traces, 48 recordings, 4 transfections), indicating that full-length BACE1 forms trimers in the plasma membrane of HEK293T cells (Fig. 2*b*). In contrast, the data were not well fit with binomial distributions for dimers (S.E.<sup>2</sup> = 80.63) and tetramers (S.E.<sup>2</sup> = 113.79), as indicated by the high S.E.<sup>2</sup> values (supplemental Fig. S2*b*). To quantify the potential participation of the ectodomain in BACE1 complex formation, we replaced the coding region of the TMS and cytoplasmic tail of msfGFP-BACE1 with the glycosylphosphatidylinositol (GPI) anchor of human placental alkaline phosphatase. This protein construct is associated with the membrane via the GPI anchor and is a well established tool to study BACE1 enzyme functions (6, 24, 25) (Fig. 2*a*). The observed step frequency distribution for BACE1-GPI was best fit (S.E.<sup>2</sup> = 4.79) with the sum of a 2nd and 4th order binomial function ( $n = 1139$  traces, 29 recordings, 3 transfections), indicating that BACE1-GPI forms dimers and that the TMS and cytosolic tail are important for trimer formation (Fig. 2*c*). The data were not well fit with binomial distributions for monomers (S.E.<sup>2</sup> =

# BACE1 trimerizes and regulates copper homeostasis

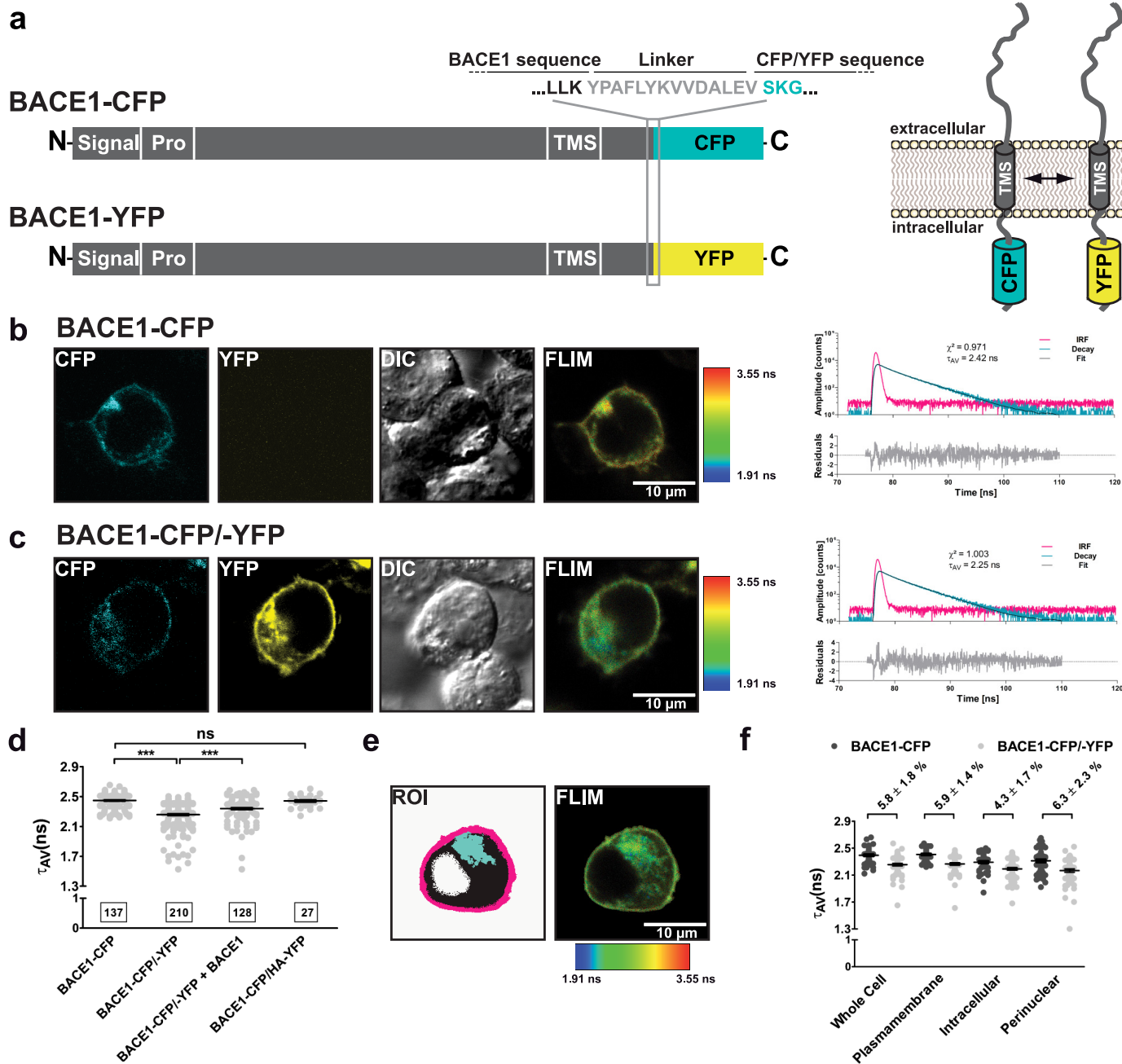


**Figure 1. Analysis of BACE1 homointeractions in living HEK293T cells.** *a*, for FLIM, BACE1 was tagged with either cyan or yellow fluorescent protein (CFP or YFP) at the C terminus. *b–f*, fluorescence lifetime of CFP was measured in transiently transfected HEK293T cells; DIC, differential interference contrast. *b* and *c*, the cyan curve depicts the fluorescence decay of CFP associated with the plasma membrane in photon counts per nanoseconds, the magenta curve is the instrument response function, and the black line is the mathematical fit. The gray curve represents the quality of the fitting. *d*, average lifetimes ( $\tau_{av}$ ) over all measured cells mean  $\pm$  S.E. (the total number of cells (*n*) is given at the bottom). Additionally, BACE1-CFP and -YFP were co-transfected with untagged BACE1 for competition. The negative control was BACE1-CFP co-expressed with influenza A virus hemagglutinin (HA)-YFP (one-way ANOVA,  $F(7,848) = 34.83$ ,  $p < 0.0001$ , Tukey's post hoc test, selected comparisons are highlighted: \*\*\*,  $p < 0.001$ ; ns,  $p > 0.05$ ). *e*, FLIM was analyzed in various ROIs: plasma membrane (magenta), perinuclear region (cyan), intracellular (dark gray). *f*, comparison of average lifetimes in different ROIs mean  $\pm$  S.E. ( $n = 62$  BACE1-CFP/-YFP,  $n = 55$  BACE1-CFP); FRET efficiencies in different ROIs in % mean  $\pm$  S.E. are indicated on top and were not significantly different (one-way ANOVA  $F(3,228) = 0.24$ ,  $p > 0.05$ ).

790.03) and trimers (S.E.<sup>2</sup> = 42.38), as indicated by the high S.E.<sup>2</sup> values (supplemental Fig. S2c). To exclude any differences in subcellular localization and/or fluorescence parameters between msfGFP-BACE1-wild-type (wt) and msfGFP-BACE1-GPI, we measured the exponential time constants ( $\tau_1$ ,  $\tau_2$ , and  $\tau_3$ ) of photobleaching, which have been previously defined as follows: coverslip contaminants ( $\tau_1$ ), msfGFP-labeled proteins

at the plasma membrane ( $\tau_2$ ), and msfGFP-labeled proteins in intracellular compartments ( $\tau_3$ ) (21). The exponential time decay constants of photobleaching were not different between msfGFP-BACE1 and msfGFP-BACE1-GPI (supplemental Fig. S2d). Similar step amplitude distributions for BACE1 and BACE1-GPI were also observed, further supporting the premise that wt and GPI-linked BACE1 were similarly localized

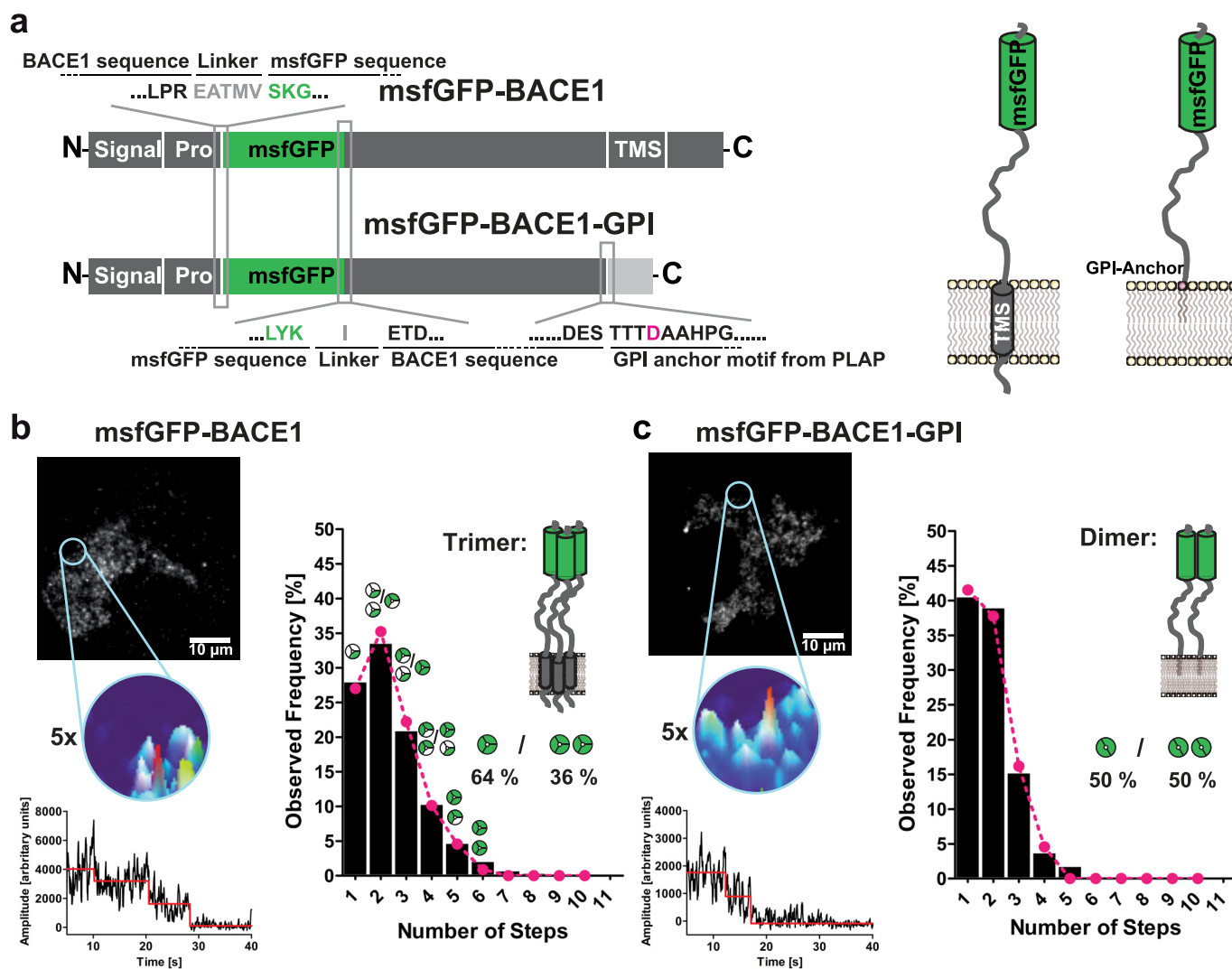


**Figure 2. Automated single-subunit counting of BACE1 in HEK293T cells.** *a*, for single subunit counting experiments, BACE1 was N-terminally tagged with the monomeric superfolder GFP (msfGFP-BACE1) (21). For msfGFP-BACE1-GPI, the coding region of the transmembrane and cytoplasmic regions were replaced by the carboxyl-terminal signal sequence of human placental alkaline phosphatase (PLAP) that links the BACE1 ectodomain through the aspartate residue, indicated in pink, to the membrane (6). *b* and *c*, bleaching steps of msfGFP fluorescence were measured in the plasma membrane of transiently transfected HEK293T cells; TIRF images (left top); inset, 3D surface plot (left middle), Chung-Kennedy filtered sample traces of single fluorophore-spot (left bottom), the red line indicates idealized bleaching steps), and a histogram of the resulting observed step frequency (right). The probability that the utilized fluorophore is fluorescent (53%) was previously determined for the imaging system that was used (21). *b*, subunit counting of BACE1 wt ( $n = 2086$  traces, 47 recordings, 4 transfections). The data were best fit ( $S.E.^2 = 7.51$ , pink dashed line) with the sum of a 3rd and a 6th order binomial function, indicating that BACE1 assembles into trimers. *c*, subunit counting of BACE1-GPI ( $n = 1139$  traces, 29 recordings, 3 transfections) and best fit ( $S.E.^2 = 4.79$ , pink dashed line) with the sum of a 2nd and 4th order binomial function, indicating that lipid-anchored BACE1 ectodomain assembles into dimers.

within the cell (supplemental Fig. S2e). Finally, to ensure that our results were not influenced by the BACE1 overexpression, the average step counts were plotted as a function of the density factor per cell for BACE1 (supplemental Fig. S2f) and BACE1-GPI (supplemental Fig. S2g); no significant correlation (Pearson  $r$ ,  $p > 0.05$ ) was found, advocating that the photobleaching step count is independent of the expression level in the cell (*i.e.* overexpression or endogenous levels of BACE1 did not confound the data *per se*).

#### Cys<sup>466</sup> is a key residue of the BACE1 trimer interface

To probe the spatial arrangement and proximity of the TMSs in BACE1 trimers, we used an advanced cross-linking approach to preserve the assembled state for subsequent analysis. We introduced a photo-cross-linkable unnatural amino acid

(*p*-azido-*L*-phenylalanine, pAzF) into different positions previously proposed to participate in its TMS interactions (14). When subjected to UV irradiation, the photoaffinity label pAzF traps even weak and transient interactions of adjacent molecules by forming covalent bonds, a powerful tool for protein cross-linking in intact cells under non-denaturing conditions (26).

BACE1 constructs with pAzF incorporated at positions Ala<sup>463</sup>, Cys<sup>466</sup>, Ala<sup>467</sup>, Leu<sup>468</sup>, and Phe<sup>469</sup> were expressed in HEK293T cells (Fig. 3a, supplemental Fig. S3, a–e). Following UV irradiation, Western blot analyses revealed BACE1 species at the expected apparent molecular weights for trimers (~191 kDa), putative dimers (~113 kDa), and non-cross-linked monomers (~58 kDa), as calculated according to the relative mobility ( $r_m$ ) of the respective marker bands, for pAzF incorporation at

## BACE1 trimerizes and regulates copper homeostasis

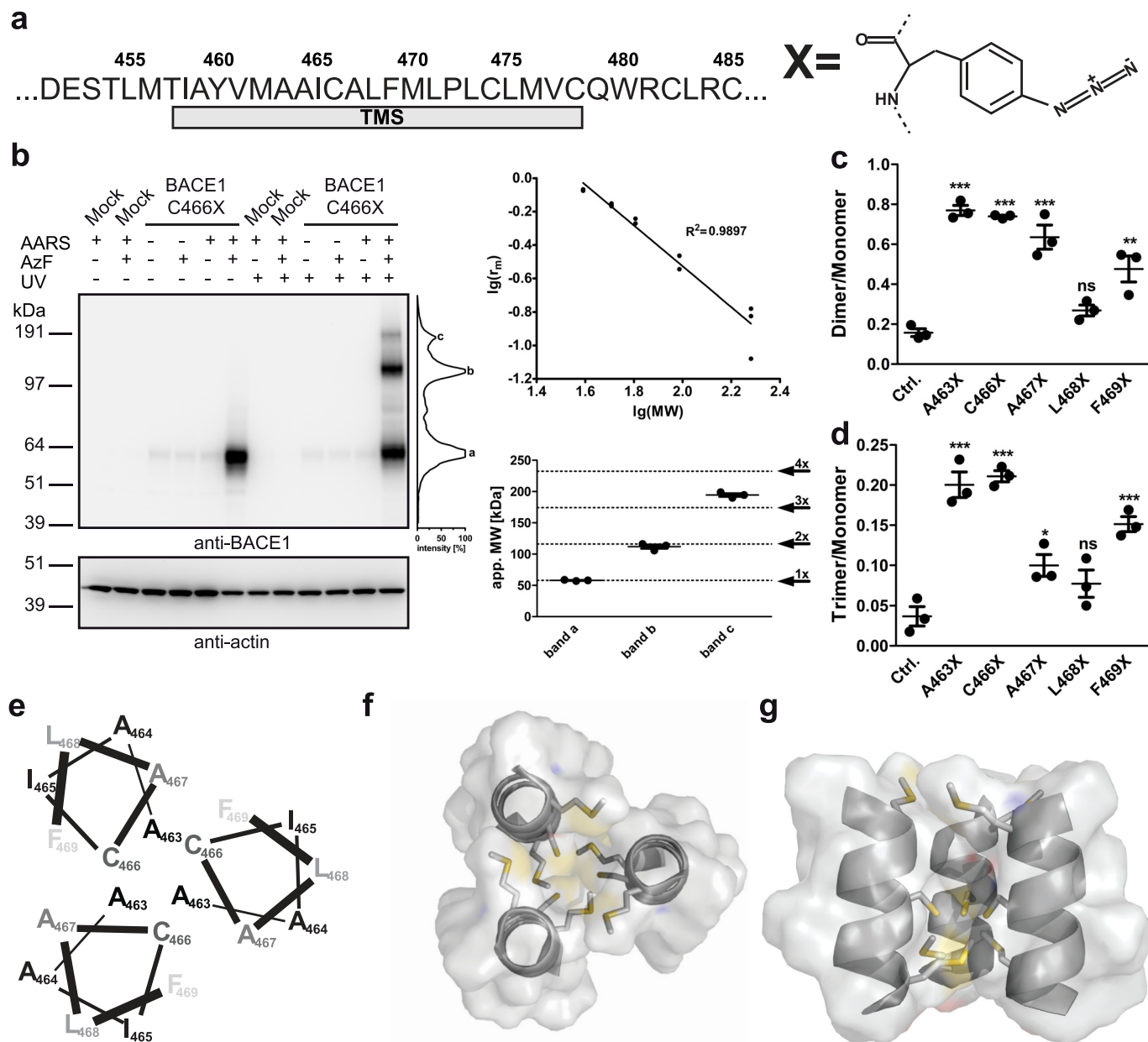


**Figure 3. Site-specific UV-cross-linking of BACE1 trimers in living HEK293T cells.** *a*, various amino acids of the BACE1-TMS were replaced by the unnatural amino acid (X) pAzF. *b*, the multimeric state of BACE1 was analyzed using Western blot analysis under reducing and denaturing conditions. Densitometry profiles of the relative abundance of cross-linked multimeric BACE1 species were analyzed using ImageJ software and are shown adjacent to the gel; actin was used as control. The decadic logarithm of the relative mobility ( $r_m$ ) of the protein standards plotted against the decadic logarithm of the apparent molecular weight between 39,000 and 191,000 kDa. The calculation of apparent molecular weight of monomeric (1 $\times$ ) BACE1 yielded 58,100 kDa. The apparent molecular weight of bands *b* and *c* correspond to the theoretical (*dashed lines*) apparent molecular weight of dimers and trimers. *c* and *d*, dimer to monomer (*c*) and trimer to monomer (*d*) band intensity ratios of BACE1. *Horizontal line* indicates the mean  $\pm$  S.E. To compare the effect of pAzF incorporation at different positions in the TMS helix relative to UV-cross-link efficiency, the data were analyzed with one-way ANOVAs and Dunnett's post hoc tests computed on the differences (compared with background signal of BACE1wt without pAzF incorporated (Ctrl.)). Dimer/monomer ratio  $F(5,12) = 39.61$ ,  $p < 0.0001$ , trimer/monomer  $F(5,12) = 28.97$ ,  $p < 0.0001$ ; Dunnett's post hoc tests (\*\*\*,  $p < 0.001$ ; \*\*,  $p < 0.01$ ; \*,  $p < 0.05$ ; ns,  $p > 0.05$ ),  $n = 3$  independent experiments. *e*, the model of relative orientation of three TMSs to one another is based on UV-cross-link efficiency (intracellular view). *f* and *g*, extracellular view (*f*) and side view (*g*) of a 3D model assuming ideal  $\alpha$ -helices (generated in PyMOL) accounting for the relative orientations shown in *e*. The central MAAICALFM sequence is displayed with side chains of sulfur-containing amino acids represented as sticks. Sulfur atoms are colored in yellow.

positions Ala<sup>463</sup>, Cys<sup>466</sup>, Ala<sup>467</sup>, and Phe<sup>469</sup>, but not Leu<sup>468</sup> (Fig. 3*b*, supplemental Fig. S3, *a–e*). Based on measured band intensities, the highest ratios of trimeric or dimeric to monomeric BACE1 forms were found for the Ala<sup>463</sup> and Cys<sup>466</sup> mutants (Fig. 3, *c* and *d*), implying that these amino acids mediate inter-helical contacts, whereas Leu<sup>468</sup>, which did not cross-link, is oriented away from the helix-helix interface. Our proposed

arrangement of the three TMSs illustrates that cross-link efficiency at different TMS positions can be very well explained by assuming a trimer interface with ideal  $\alpha$ -helices (Fig. 3*e*). Based upon this spatial orientation, we constructed a 3D model indicating that the interaction site between the helices is lined by the sulfur-containing residues Met<sup>462/470</sup> and Cys<sup>466</sup> (Fig. 3, *f* and *g*). Our 3D model predicts that this sulfur-rich core could

thus be accessible and act as a metal ion interaction site in the cellular context.

To validate our model and to test whether cysteines in the BACE1 TMS are in close proximity we performed chemical cross-linking experiments. We employed a previously developed cross-linking protocol, using  $\text{HgCl}_2$ , which rapidly and selectively bridges vicinal pairs of sulfhydryl groups to form intermolecularly linked mercury dimers (27, 28). Our results show that two subunits within the BACE1 trimer can be cross-linked by mercury, whereas BACE1 C466A fails to undergo this reaction (supplemental Fig. S4). This indicates that the cross-link requires the presence of the sulfhydryl group of Cys<sup>466</sup> and that the mercury-induced cross-link occurs at this specific position. Additionally, we tested whether Ag(I) could coordinate more than two BACE1 subunits of the BACE1 trimer complex via Cys<sup>466</sup>. Using  $\text{AgNO}_3$  in the same experimental protocol, we found that three BACE1 subunits can be specifically cross-linked via Cys<sup>466</sup> (supplemental Fig. S4). Overall, our results indicate that the TMSs in full-length cellular BACE1 form a trimer interface, where the central Cys<sup>466</sup> residues are adjacent to one another.

#### Copper ions are dispensable for BACE1 trimerization and BACE1-APP interactions

We found in our previous study, using synthetic peptides covering the TMS, that the sulfur-rich core of the BACE1 TMS, Met<sup>462</sup>-XXX-Cys<sup>466</sup>-XXX-Met<sup>470</sup>, can act as a Cu(I)-binding site, with Cys<sup>466</sup> being absolutely required for copper-complex formation (14). To test the effect of Cu(I) on the native cellular structure of BACE1, *i.e.* trimerization, we performed additional subunit counting experiments with BACE1 constructs in the absence and presence of the high-affinity Cu(I) chelator bathocuproine disulfonate (BCS,  $\log\beta_2 = 20.8$  (29)).

Wt BACE1 yielded similar trimeric outcomes in the presence (Fig. 2b) and absence (Fig. 4a) of endogenous copper ions. Specifically, the observed step frequency distribution of BCS-treated msf-GFP-BACE1 ( $n = 1568$  traces, 47 recordings, 3 transfections) was best fit ( $\text{S.E.}^2 = 18.70$ ) with the sum of a 3rd and 6th order binomial function. The Cys<sup>466</sup> mutant also formed trimers and independently of the BCS copper chelator (Fig. 4, b and c). Specifically, the histogram of the observed step frequency distribution for msf-GFP-BACE1 C466A ( $n = 1224$  traces, 26 recordings, 3 transfections) was best fit ( $\text{S.E.}^2 = 21.67$ ) with the sum of a 3rd and 6th order binomial function (Fig. 4b). Likewise, the histogram of the observed step frequency distribution for BCS-treated msf-GFP-BACE1 C466A ( $n = 1512$  traces, 32 recordings, 3 transfections) was best fit ( $\text{S.E.}^2 = 15.94$ ) with the sum of a 3rd and 6th order binomial function (Fig. 4c). Taken together, our subunit counting data and complementary FLIM-FRET analyses (supplemental Fig. S5) demonstrate that the formation of BACE1 trimers is independent of Cys<sup>466</sup> and Cu(I)-ions in living HEK293T cells. This finding implies that copper ions do not trigger trimerization through Cys<sup>466</sup> or other possibly undetermined binding sites of BACE1.

To test the effect of copper on APP processing (Fig. 4, d–h), we used HEK293T cells transiently co-transfected with APP wt, BACE1, and BACE1 C466A, respectively (Fig. 4e). A slight

decrease in full-length APP levels, a concomitant increase in  $\beta$ -C99 and  $\beta'$ -CTF (C89), and a decrease in the  $\alpha$ -secretase product  $\alpha$ -CTF (C83) were detected upon BACE1 or BACE1 C466A transfection, when cell growth and *de novo* synthesis of proteins were prevented with cycloheximide (to block translational elongation) after copper treatment (Fig. 4, e and f). The levels of secreted sAPP $\alpha$  and sAPP $\beta'$  (as detected by mAb W02, which does not differentiate between the two forms; see Fig. 4f) were found markedly decreased in conditioned media of BACE1 and BACE1 C466A expressing cells. Note that sAPP $\beta$  was not detectable in the absence of BACE1, only under BACE1-overexpression conditions (Fig. 4f). Interestingly, copper treatment elevated the levels of sAPP $\alpha$  and sAPP $\beta'$  in the absence of overexpressed BACE1 (as previously described for sAPP $\alpha$  (30)), but had no effect on sAPP $\alpha$  and sAPP $\beta'$  or sAPP $\beta$  when it was overexpressed (Fig. 4f). To determine the relative amounts and to differentiate between sAPP forms generated by  $\alpha$ -secretase or BACE1, we performed ELISAs with the conditioned media (Fig. 4, g and h). In APP-only transfected HEK293T cells, considerable amounts of sAPP $\alpha$  were secreted into the media, whereas sAPP $\beta$  was at the detection limit (Fig. 4, g and h). Copper treatment significantly elevated the levels of sAPP $\alpha$  (30), indicating an altered APP cleavage at the  $\alpha$ -secretase site (Fig. 4g). Both co-expression of APP plus BACE1 wt and APP plus BACE1 C466A yielded a marked increase in sAPP $\beta$ , which was neither different between BACE1 wt and BACE1 C466A, nor affected by copper treatment (Fig. 4h). Together, these results suggest that neither copper nor the mutation C466A affect APP processing by BACE1. In summary, these data further substantiate our model that native BACE1 predominantly exists as a naturally membrane-bound trimer.

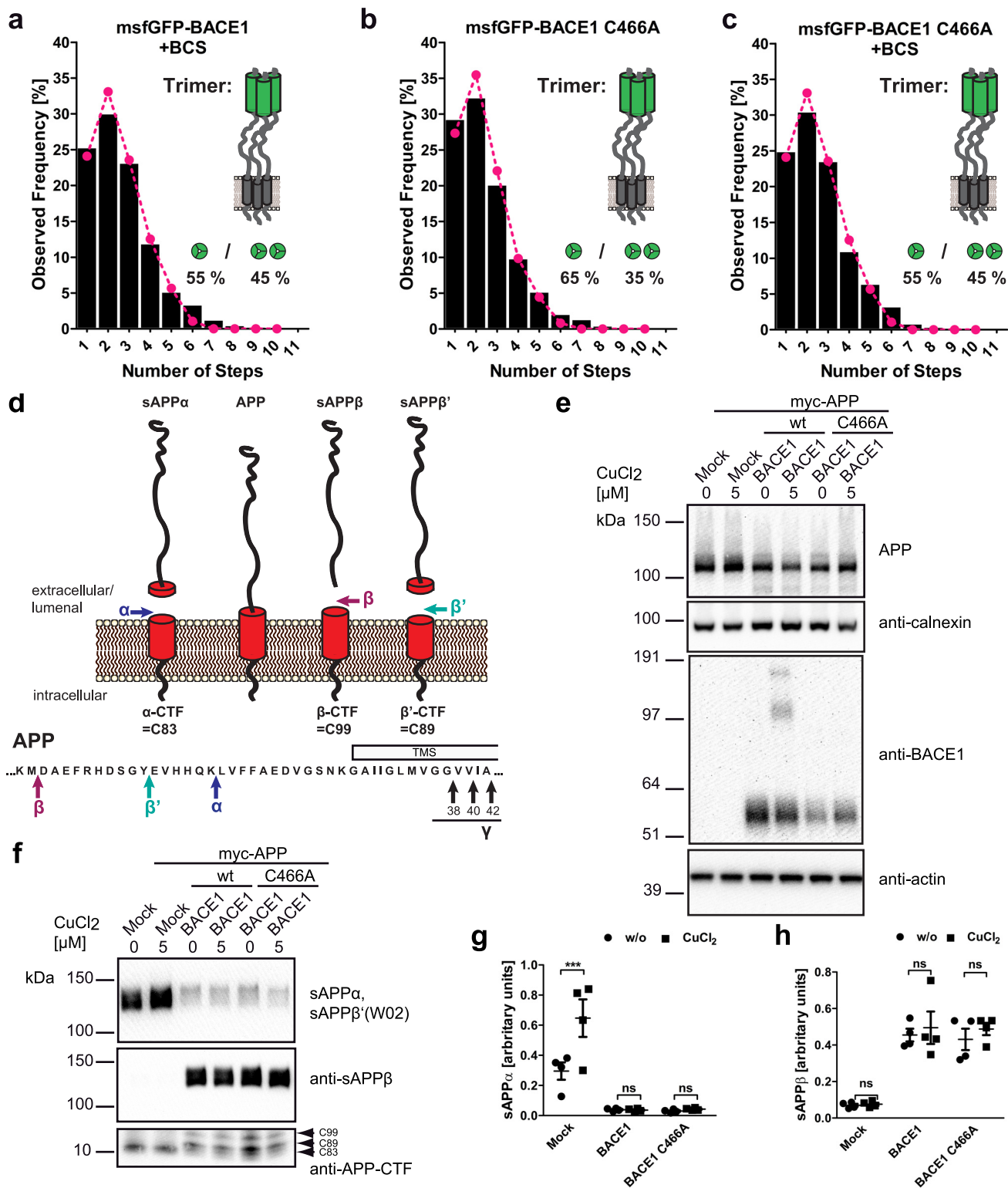
#### BACE1 modulates cytosolic copper levels

BACE1 cycles between the plasma membrane, endosomes, and the trans-Golgi network (31). To test a potential role of endogenous BACE1 in maintaining cellular copper homeostasis, we analyzed whether endogenous BACE1 affects intracellular copper compartmentalization. We utilized a metal-responsive element (MRE) luciferase reporter assay to monitor cytoplasmic copper (supplemental Fig. S6a) (32). It allows to monitor cytosolic copper bioavailability with respect to BACE1 expression. By comparing BACE1 to the P-type ATPase Atp7b, we assessed the potential role of BACE1 in cellular copper homeostasis. Atp7b was described to directly pump copper from the cytosol to the cell exterior (33), or to have a role in the intracellular compartmentalization of copper, depending on the cell type and specific splice variant expressed (34). Interestingly, the siRNA-mediated knockdown of endogenous BACE1 in HEK293T cells increased cytoplasmic copper bioavailability 3–4-fold (Fig. 5a), which strongly agrees with the robust reduction of BACE1 protein levels after 48 h (supplemental Fig. S6b). The Atp7b knockdown surprisingly increased cytoplasmic bioavailability to a similar extent (4-fold; Fig. 5a) with a comparable reduction in protein levels (supplemental Fig. S6b). In complementary assays, we analyzed a possible influence of BACE1 enzyme activity on cytosolic copper levels. In the presence of the well characterized BACE1-specific cell-permeable inhibitor

## BACE1 trimerizes and regulates copper homeostasis

IV ( $IC_{50} = 15 \text{ nM}$ ) (35), cytosolic copper levels remained unaffected (Fig. 5a). This implies that enzymatic activity and the postulated function of BACE1 in copper homeostasis must be independent of each other. We also tested whether the BACE1 C466A mutant could attenuate the increase in cytosolic copper when endogenous BACE1 was knocked down. Indeed, overexpression of knockdown-resistant wt BACE1 resulted in a partial

reversal of cytosolic copper increase, whereas the C466A mutant completely failed to rescue the effect, as revealed by transfections of empty plasmid (Mock), BACE1, or BACE1 C466A on either siRNA-BACE1 or scr-siRNA backgrounds (Fig. 5b; see supplemental Fig. S6c for expression levels). These data suggest that BACE1 and Atp7b may have related functions in copper homeostasis in HEK293T cells. To further test this



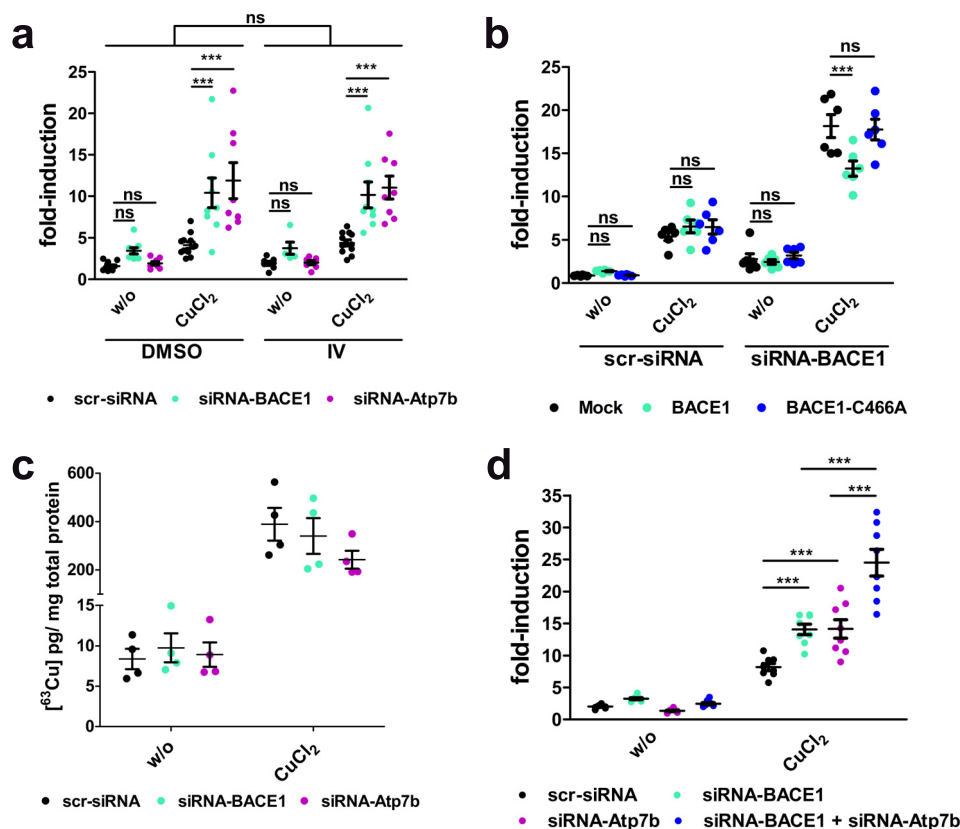


**Figure 5. Analysis of endogenous BACE1 in the regulation of cytosolic copper levels.** *a*, analysis of cytosolic copper after siRNA-mediated knockdown of endogenous BACE1, or inhibition of BACE1 activity by the specific inhibitor IV in HEK293T cells. Fold-induction was calculated by normalizing to no siRNA transfection and vehicle (DMSO) treatment. *b*, analysis of cytosolic copper of cells expressing exogenous BACE1 and BACE1 C466A on the background of siRNA transfection and no copper treatment,  $n = 6$  independent experiments. *c*, quantification of total cellular copper by inductively coupled plasma mass spectrometry (ICP-MS),  $n = 4$  independent experiments. *d*, analysis of cytosolic copper after siRNA-mediated knockdown of endogenous BACE1 and/or Atp7b in HEK293T cells. Fold-induction was calculated by normalizing to no siRNA transfection;  $n = 8$  independent experiments. *a–d*, data are shown as mean  $\pm$  S.E. The data were analyzed with between subject two-way ANOVAs, significant interactions were followed-up with simple main effects and Bonferroni post hoc tests; \*\*\*,  $p < 0.001$ ; ns,  $p > 0.05$  (see also supplemental Fig. S6f).

hypothesis, we quantified total cellular copper levels by inductively coupled plasma mass spectrometry (ICP-MS). Notably, neither BACE1-deficient, nor Atp7b-deficient cells had altered levels of total cellular copper (Fig. 5c, see supplemental Fig. S6d for expression levels). These results indicate that endogenous BACE1 may have a role in transferring cytosolic copper to intracellular compartments rather than in the cellular export of copper. To gain further mechanistic insight into how BACE1 affects cellular copper compartmentalization, we tested whether the effects of BACE1 and Atp7b are additive. We found that cells that are deficient in BACE1 and Atp7b had significantly higher cytosolic copper levels, compared with the individual knockdowns or controls (Fig. 5d; see supplemental Fig. S6e for expression levels). These findings suggest that

BACE1 and Atp7b have related yet independent functions in cellular copper homeostasis.

## Discussion

The present study provides direct evidence that full-length BACE1 forms trimers in biological membranes of live cells, and that BACE1 requires its unique transmembrane sequence to properly build a stable homotrimeric subunit organization. We used automated single-subunit counting (21) to show that BACE1 is a trimeric integral membrane protein in the plasma membrane of HEK293T cells (Fig. 2). Because our FLIM-FRET results indicated that BACE1 homointeractions are independent of the subcellular localization, we anticipate that BACE1 trimers are not only present at the plasma membrane but

**Figure 4. Analysis of copper effects on BACE1 trimerization and BACE1-APP interactions.** *a–c*, subunit counting histograms of BCS-treated msf-GFP-BACE1 (*a*,  $n = 1568$  traces, 47 cells, 3 transfections, best fit  $S.E.^2 = 18.70$ ), msf-GFP-BACE1 C466A (*b*,  $n = 1224$  traces, 26 cells, 3 transfections, best fit  $S.E.^2 = 21.67$ ), and BCS-treated msf-GFP-BACE1 C466A (*c*,  $n = 1512$  traces, 32 cells, 3 transfections, best fit  $S.E.^2 = 15.94$ ) expressing cells. In all cases, the observed step frequency distributions were best fit with the sum of a 3rd and 6th order binomial function, indicating trimer formation. *d–h*, HEK293T cells were co-transfected with APP695wt and BACE1 or BACE1 C466A, respectively. Data were collected from 4 independent experiments. *d*, schematic representation of soluble fragments and CTFs resulting from ectodomain shedding of APP by  $\alpha$ -secretase or BACE1. APP is cleaved into sAPP $\alpha$  and  $\alpha$ -CTF by  $\alpha$ -secretase, sAPP $\beta$ , and  $\beta$ -CTF or alternatively sAPP $\beta'$  and  $\beta'$ -CTF by  $\beta$ -secretase (BACE1). Cleavage sites within the APP sequence are indicated in the bottom panel. C-terminal fragments are further processed by  $\gamma$ -secretase at the indicated positions and yield fragments ending at amino acid position 38, 40, and 42 (A $\beta$ -numbering). *e* and *f*, representative Western blots for the examination of APP695 and BACE1 expression (*e*) and APP-cleavage products from cell culture supernatants sAPP $\alpha$ /sAPP $\beta'$  (*top*), sAPP $\beta$  (*middle*), and C-terminal fragments from lysates (*bottom*) (*f*). *g* and *h*, quantification of sAPP $\alpha$  (*g*) and sAPP $\beta$  (*h*) in cell culture supernatants with specific ELISAs. *g*, one-way ANOVA,  $F(5,18) = 19.94$ ,  $p < 0.0001$ ; *h*, one-way ANOVA,  $F(5,18) = 18.23$ ,  $p < 0.0001$ , Tukey's post hoc test, \*\*\*,  $p < 0.001$ ; ns,  $p > 0.05$ .

## BACE1 trimerizes and regulates copper homeostasis

assemble in intracellular/perinuclear compartments (Fig. 1). When the BACE1 ectodomain was expressed as an engineered GPI-anchored molecule without the TMS, it could only assemble into dimers (Fig. 2c). This finding is of special interest, because it has been previously demonstrated that BACE1-GPI cleaves APP to a lesser extent at the  $\beta'$ -site (6). Together, it could be speculated that only trimeric (but not dimeric) BACE1 harbors the ability to specifically cleave at this site. However, alternative explanations, as pointed out in the original study by Vetrivel *et al.* (6), *i.e.* structural changes to the ectodomain introduced via the GPI-anchor modification, are similarly plausible. Furthermore, we validated our concept of BACE1 trimers at the TMS level by *in vitro* in-cell cross-linking, *i.e.* introduction of the unnatural, UV-activatable amino acid pAzF at specific positions in the TMS and chemical cross-linking of BACE1 via Cys<sup>466</sup> (Fig. 3, supplemental Figs. S3 and S4). These cross-linking experiments, followed by denaturing SDS-PAGE, enabled the detection of intersubunit interactions in BACE1 trimers that are reflective of the cellular situation and furthermore, provided positional information about the interface. Here, our results revealed that the detection of cross-linked trimers depends on the specific position of pAzF in the TMS. The successful cross-link at four different positions in the BACE1 TMS (Ala<sup>463</sup>, Cys<sup>466</sup>, Ala<sup>467</sup>, and Phe<sup>469</sup>) and the low trimer:monomer ratios of the other position (Leu<sup>468</sup>) tested, suggest a model where the four amino acids participate in inter-helical contacts along an inner  $\alpha$ -helical axis surface of the trimeric assembly (Fig. 3d). Thus, the cross-linking data further supports the existence of native trimers in cells, although due to imperfect cross-linking efficiency, monomers, dimers, and trimers were detected in cells. Our chemical cross-linking experiments of BACE1 via Cys<sup>466</sup> demonstrated an increased cross-linking efficiency (supplemental Fig. S4), which support the idea of the trimeric state being the preferred cellular stoichiometry of BACE1. Together, our current study suggests a model in which the contact site encompasses the sulfur-rich core sequence motif with the central residue Cys<sup>466</sup> and the outside lateral edges formed by Met<sup>462</sup> and Met<sup>470</sup> (Fig. 3, f and g).

Because Cys<sup>466</sup> is part of the helical contact site detected by our cross-linking data and we found previously that this residue is indispensable for the Cu(I) interaction of the sulfur-rich core of the BACE1 TMS (14), we tested whether the trimer formation of full-length BACE1 in living cells occurred independently of Cu(I) and Cys<sup>466</sup> (Fig. 4). Neither Cu(I) nor Cys<sup>466</sup> are necessary to support cellular trimerization of full-length BACE1 because it remained unaltered by Cu(I) depletion with BCS and when Cys<sup>466</sup> was replaced. Furthermore, the enzymatic activity of BACE1 toward its substrate APP was unchanged upon copper treatment or mutation of Cys<sup>466</sup> (Fig. 4). Our analysis showed that neither condition affected the production of sAPP $\beta$ , sAPP $\beta'$ ,  $\beta$ -CTF (C99), or  $\beta'$ -CTF (C89), the direct products of BACE1-mediated APP-cleavage. Although copper treatment had no effect on BACE1-mediated APP shedding we do not exclude the possibility that Cu(I) binding to the BACE1 TMS could potentially affect the processing of other BACE1 substrates.

Previous studies by us and others suggest that BACE1 could have a function in copper homeostasis, *e.g.* BACE1 was found to interact with the copper chaperone for superoxide dismutase-1

(SOD1) and to bind copper ions via its sulfur-rich TMS (9, 14). In fact, we now show that the relative orientation of the TMS helices within the BACE1 trimer is such that the copper-binding residues are oriented toward the inner surface (Fig. 3, f and g). It may be considered necessary if ions like Cu(I) are transported across membranes through a channel-like arrangement of the three BACE1 helices. Thus, our model is reminiscent of the newly identified soluble copper storage protein (Csp1), which forms a four-helix bundle binding multiple Cu(I) ions within an established protein-folding motif via Cys residues that point into the core of the bundle (36). Our concept of BACE1 having a role in copper homeostasis is strongly supported by our findings with HEK293T cells deficient in BACE1 protein. Surprisingly, such cells accumulated large amounts of copper in the cytosol to the same degree as Atp7b-deficient cells (Fig. 5). Moreover, BACE1 and Atp7b-deficient cells did not show a change in total cellular copper levels. Typically, Atp7b exports copper from the cytoplasm into the lysosomal lumen for further exocytosis (33), however, endogenous Atp7b in HEK293T cells does not localize to the plasma membrane or lysosomal compartments and is thought to transport copper into cytoplasmic storage compartments (34). Consistent with recent reports that lysosomes effectively export copper using Atp7b in response to rising copper levels in hepatocytes (33), we propose that BACE1 operates to sequester excess copper into non-secretory organelles. Our observation that BACE1 exogenously expressed in BACE1-deficient HEK293T cells partially restored the intracellular copper levels, whereas the mutant BACE1 C466A failed to do so and was indistinguishable from control, further supports this view. The surprisingly similar behavior of endogenous BACE1 and Atp7b in cellular copper compartmentalization led us to explore whether their regulatory effects act in concert or independent of one another. Our results demonstrated that cells deficient in BACE1 and Atp7b accumulated significantly larger amounts of cytosolic copper than cells that are only deficient in one of them (Fig. 5). Thus, both endogenous BACE1 and Atp7b are necessary for the maintenance of cellular copper compartmentalization, however, they act in independent pathways and additively affect cytosolic copper levels. In contrast to animals lacking Atp7b function (37, 38), BACE1-deficient mice have not been reported to display apparent signs of copper imbalance (1). However, the effect of BACE1 on copper distribution *in vivo* might be subtle and not immediately obvious, similarly to previously observed effects of inactivation/elimination of individual copper-binding proteins (17, 39).

How can our current results be integrated into a model? We suspect that BACE1 helps maintain cytosolic copper levels and even plays a role in copper detoxification under conditions of high cytosolic copper levels. Mechanistically, we propose that BACE1 binds metal ions from the cytoplasm with the help of copper chaperones and transports Cu(I) using Cys/Met clusters of the Met<sup>462</sup>-XXX-Cys<sup>466</sup>-XXX-Met<sup>470</sup> motif of the TMS into cytoplasmic compartments. In general, copper-trafficking pathways are highly evolved networks where binding affinities have been fine-tuned to promote transfer of the metal ion to a recipient protein (40, 41). Similarly to Atp7b in renal cells (34), BACE1 could maintain cytosolic copper levels by sequestering

copper in the ER, Golgi, trans-Golgi network, endosomes, and/or lysosomes.

Ultimately, our findings raise concerns regarding treatment strategies aimed at the suppression of enhanced BACE1 expression, because adverse effects in cellular copper homeostasis may be expected. However, the exact mechanism underlying the role of BACE1 in the cellular copper transport system must await confirmation.

## Experimental procedures

### Plasmids, mutagenesis, and siRNA

A human BACE1 construct (full-length BACE1, isoform A; pcDNA3.1+/Zeo; Invitrogen) described earlier (42) was used for expression and modified according to the requirements. To obtain BACE1 constructs with C-terminal CFP or YFP fusion, custom made pcDNA3+/G418-CFP and -YFP constructs were converted into Gateway compatible vectors (Gateway Vector Conversion System, Invitrogen). For msfGFP constructs, BACE1 was subcloned from pcDNA3.1+/Zeo into pRK5. BACE1-fusion vectors were generated by inserting the cDNA coding for the fluorescent monomeric superfolder green fluorescent protein (msfGFP-V206K referred to simply as msfGFP in the text) after the region coding for the propeptide and before the region encoding mature full-length BACE1. A silent NruI restriction site was created followed by a blunt-blunt ligation of the sequence coding for msfGFP. To replace the coding region of the transmembrane domain and cytoplasmic tail of msfGFP-BACE1, a double-stranded, sequence-verified gene fragment (gBlock, IDT) coding for the glycosylphosphatidylinositol-anchor region from human placental alkaline phosphatase was used to replace the corresponding region (using PvuII- and HindIII-restriction sites).

Plasmid pSVB.Yam encoding an amber suppressor tRNA derived from the *Bacillus stearothermophilus* Tyr-tRNA and *Escherichia coli* aminoacyl-tRNA synthetase Tyr-RS-pAzF with a C-terminal FLAG tag in pcDNA3.1(+) were used previously (43, 44) and were a kind gift from Thomas Sakmar (Rockefeller University). Plasmids pGL3-E1b-TATA-4MRE and pRL-TK vector (Promega Benelux BV) were used previously (32) and were a kind gift from Leo Klomp (University Medical Center Utrecht). The cDNA encoding APP695 wt with an N-terminal myc-tag was subcloned from pCEP4 (Invitrogen) (45) in the pcDNA3.1+/Zeo vector (Invitrogen).

To create knockdown-resistant BACE1 and BACE1 C466A, the region CGAATTGGCTTTGCTGTC coding for RIGFAV, which is targeted by siRNA-BACE1, was replaced using a g-block containing the sequence AGGATCGGTTTCGCCGTA (coding also for RIGFAV). The g-block was inserted using BspMI and XhoI restriction sites. Point mutations were introduced by site-directed mutagenesis, using either a QuikChange Kit (Stratagene/Agilent) or PfuUltra II Fusion HS (Stratagene/Agilent) followed by DpnI (New England Biolabs) digestion. All constructs were verified by DNA sequencing. For knockdown experiments, siGENOME NonTargeting siRNA No. 3 (scr-siRNA), siGENOME BACE1 siRNA NCBI Probe Id 12226196 (siRNABACE1), and si-GENOME Atp7b siRNA

NCBI Substance Id 135615821 (siRNA-Atp7b) (all from Dharmacon) were used.

### Cell culture and transfections

HEK293T (DSMZ number ACC 305) cells were grown in DMEM (high glucose (4.5 g/liter), 10% fetal bovine serum (FBS), 2 mM glutamine, 1 mM pyruvate) in a humidified incubator at 37 °C 5% CO<sub>2</sub>. Cells were routinely tested for mycoplasma contamination. For single subunit counting experiments, HEK293T cells were cultured in DMEM containing 2–3% FBS. For transient transfection, cells were seeded on poly-D-lysine-coated (Sigma) 10-cm 6- and 24-well plates (Fisher) and transiently transfected 20–24 h later by using TransFectin (or RNAiMax, when only siRNA was used) according to the manufacturer's protocol (Bio-Rad/Invitrogen).

### Western blot analysis

Cell culture supernatants were removed and centrifuged at 450 × g in a microcentrifuge (Eppendorf) at 4 °C for 10 min to remove potential cell contamination. Cells were washed once on ice with ice-cold PBS containing Ca<sup>2+</sup> and Mg<sup>2+</sup> (PBS<sup>2+</sup>) and lysed in 20 mM Tris-HCl, pH 7.5, 150 mM NaCl, 20 mM CHAPS, 2 mM phenylmethylsulfonyl fluoride (PMSF), 2× Complete protease inhibitor (Roche Applied Science), for 60 min at 4 °C. Lysates were centrifuged at 10,621 × g in a microcentrifuge (Eppendorf) at 4 °C for 15 min to remove the nuclear fraction. Lysates were subjected to colorimetric protein determination using a bicinchoninic acid assay (BCA assay, Pierce), according to the manufacturer's protocol. Equal protein amounts were brought to the same volumes with lysis buffer and LDS loading buffer (Invitrogen) with or without dithiothreitol (DTT) was added to the samples. Media loading was normalized to lysate protein concentration. Samples were heated to 70 °C for 10 min and proteins were separated on 8% Tris glycine gels, 10–20% Tris-Tricine (Bio-Rad), or 4–12% BisTris gradient gels (Invitrogen). Proteins were transferred onto polyvinylidene difluoride (PVDF) (Millipore) or nitrocellulose membranes (Bio-Rad) by tank blotting (Bio-Rad) at 4 °C.

### Antibodies and immunodetection

BACE1 was detected with polyclonal EE-17 (Sigma) or monoclonal D10E5 (Cell Signaling), APP with the monoclonal 22C11 (Millipore), sAPPβ by the polyclonal anti-sAPPβ antibody (IBL, Japan), sAPPα and sAPPβ' by the monoclonal W02 (Millipore), Atp7b by the monoclonal EPR6794 (Abcam), actin by the monoclonal mab1501 (Millipore), calnexin by the monoclonal MAB3126 (Millipore), GFP by the monoclonal anti-GFP ABfinity (Invitrogen), and APP-CTFs by the polyclonal AB5352 (Millipore). BACE1, Atp7b, and CTFs were also immunoprecipitated with the monoclonal MAB9311 (R&D Systems), polyclonal PA1–16583 (Pierce), and the polyclonal 27576 raised against synthetic APP-(648–695) (46), respectively.

Secondary antibodies were anti-mouse- and anti-rabbit-HRP, respectively (Promega), or anti-rabbit light-chain-HRP (Jackson). Signals were recorded on ImageQuant LAS 500 (GE Healthcare Life Sciences) or the FluorChem FC2 (Alpha Innotech).

## BACE1 trimerizes and regulates copper homeostasis

### Confocal microscopy and FLIM-FRET imaging

HEK293T cells were incubated in BBS buffer (20 mM BisTris-HCl, 137 mM NaCl, 27 mM KCl, 10 mM CaCl<sub>2</sub>, 5 mM MgCl<sub>2</sub>, pH 6.8 (all chemicals were purchased from Roth, Germany) for imaging. Intensity measurements as well as FLIM-FRET measurements were performed as described before (47). Measurements were carried out using an inverted FluoView 1000 microscope (Olympus, Tokyo, Japan) equipped with a time-resolved LSM Upgrade kit (PicoQuant, Berlin, Germany) and a  $\times 60$  oil immersion objective (1.35 numerical aperture) at 25 °C. FLIM was used to study energy transfer between the BACE1-CFP (donor) and BACE1-YFP (acceptor). CFP was excited at 440 nm using a laser diode and detected in the range of 460 to 490 nm. YFP was excited at 515 nm using an argon laser and detected in the range of 535 to 575 nm. Fluorescence intensities of the donor and acceptor were analyzed with ImageJ. FLIM images of the donor in the absence and presence of acceptor were acquired upon excitation of the donor at 440 nm using a pulsed laser diode. Fluorescence was detected by a single photon avalanche photodiode and a  $470 \pm 15$ -nm bandpass filter. Electrical signals were processed by using the TimeHarp 200 PC card. Analysis of FLIM images was performed using Sym-PhoTime software (PicoQuant), taking into account the instrument response function. FLIM pictures were accumulated for 90 s (60 frames with an average photon count rate of  $2-8 \times 10^4$  counts/s). The measured photons-per-pixels for pixels corresponding to the plasma membrane or other regions of interest were combined into a decay curve that was further analyzed by fitting it using a non-linear least squares iterative procedure as the sum of two exponential terms. This kind of fitting is required because fluorescent protein variants are known to show a multiple exponential decay (48). Biexponential fitting was carried out as previously described by Scolari *et al.* (49). For every cell, the average lifetime ( $\tau_{av}$ ) of CFP was calculated using the equation  $\tau_{av} = \sum_i \alpha_i \tau_i$  with the fluorescence lifetimes  $\tau_i$  and the respective amplitudes  $\alpha_i$ .

### Single-molecule fluorescent subunit counting

Subunit counting was performed essentially as described previously (21). A total of 62,500 cells/dish were plated on poly-D-lysine-coated 35-mm glass-bottom (No.1) MatTek dishes 24–28 h prior to transfection. Transfection was performed by calcium phosphate precipitation (21). After transfection, HEK293T cells were allowed to recover between 12 and 18 h (in the presence or absence of the Cu(I)-chelator BCS (Sigma)) before being fixed using 4% EM-grade formaldehyde (Ladd Research) in PBS for 24–48 h at 4 °C. Data were acquired at rate of 20 Hz under TIRF illumination using a  $128 \times 128$  backlit EMCCD camera (iXon+ 860BV, Andor Technology, South Windsor, CT) with a  $\times 60/1.49$  NA objective (Olympus, Richmond Hill, Canada) coupled to a Zeiss Axiovert 200 microscope. Photobleaching illumination intensity was set to 500  $\mu$ W (measured through the objective) from a 60-milliwatt 488-nm laser (PhoXx, Omicron-Laserage, Germany). Data analysis was performed using the automated software package Progressive Idealization and Filtering (21). Due to the system resolution, the selection of spots to be included for analysis was

limited to a maximum of 1 neighbor (*i.e.*  $3 \times 3$  pixel spot size) containing an absolute minimum fluorescence intensity of 1750 AU and a minimum signal-to-noise ratio ( $dF/F$ ) of 10%. The spot overlap limit was restricted to a  $\sigma$  of 1.25. Traces were filtered using a single-pass Chung-Kennedy filter with a window size of 3. Step detection parameters were as follows: minimum step length of 3 frames, amplitude tolerance of 60%, and minimum step amplitude of 375 AU. Trace quality control parameters were as follows: minimal step signal-to-noise value of 2.5, counter-fit/fit ratio of 1.0, maximum allowable  $\chi$ -squared ( $\chi^2$ ) fit of 1.5, total fluorophore photobleach length of 90%, and a maximum step amplitude of 2550 AU. Inset surface plots were created in ImageJ using the Interactive 3D Surface Plot plug-in (Kai Uwe Barthel author).

The  $p_m$  value, reflecting the probability that the utilized fluorophore is fluorescent, was required to be within 0.49 and 0.56. The  $p_m$  value has previously been determined to be 0.53 (for the same imaging system, cell type, and culturing conditions that we used for our BACE1 analysis) (21) and is an intrinsic property of the msfGFP.  $p_m$  remained stable at the value 0.53 for all msfGFP published and unpublished fusion proteins used to date (21). To illustrate that the observed step frequency distribution for BACE1 and BACE1-GPI would yield  $p_m$  values within the required range between 0.49 and 0.56, we fitted the histogram of the observed step frequency distribution for BACE1 (supplemental Fig. S7a) and BACE1-GPI (supplemental Fig. S7b) with a free-floating  $p_m$ . We obtained  $p_m = 0.50$  for trimeric BACE1 and  $p_m = 0.56$  for dimeric BACE1-GPI. Note that the step frequency distribution for BACE1 and BACE1-GPI would also fit well for higher oligomeric states for  $p_m$  values lower than 0.49, which is outside the required range and therefore unlikely to exist (supplemental Fig. S7, *a* and *b*).

### Incorporation and UV-cross-link of unnatural amino acids

After transfection, HEK293T cells were treated with 0.5 mM pAzF. pAzF was dissolved in 1 M NaOH at a concentration of 100 mM. pAzF (final concentration of 0.5 mM) was added from this stock solution to culture medium and neutralized with 37% HCl. Medium was replaced 6, 24, 48, and 72 h post-transfection. 96 h post-transfection cells were washed on ice with ice-cold PBS<sup>2+</sup> and cross-linked on a standard lab UV table (2.0 W/cm<sup>2</sup>) for 30 min at 4 °C in 1.5 mM CaCl<sub>2</sub>, 1.5 mM MgCl<sub>2</sub>, 5 mM HEPES, 1 mg/ml of glucose in PBS, pH 7.4.

### Chemical cross-link of cysteines

For HgCl<sub>2</sub> (20  $\mu$ M) and AgNO<sub>3</sub> (50  $\mu$ M) treatments (10 min at room temperature), cells were washed and treated in 2.5 mM CaAcOH, 2.5 mM MgAcOH, 20 mM HEPES, 230 mM sucrose, pH 7.4, analogously to a previously described protocol (28). Before lysis, cells were incubated with 20 mM *N*-ethylmaleimide.

### Cell-based BACE1 activity assay

Cells were co-transfected with BACE1 (wt or C466A) and APP695 wt encoding constructs. The cells were washed 18 h post-transfection with PBS<sup>2+</sup> and treated with CuCl<sub>2</sub> in artificial CSF (142 mM NaCl, 5 mM KCl, 10 mM glucose, 1 mM MgCl<sub>2</sub>, 2 mM CaCl<sub>2</sub>, and 10 mM HEPES at pH 7.4) in a 37 °C incubator

for 60 min (all chemicals from Sigma). ACSF was replaced by Opti-MEM (Invitrogen) containing 10  $\mu\text{g}/\text{ml}$  of cycloheximide (Sigma) to block *de novo* protein synthesis. Cell supernatants were conditioned for 8 h and subjected to sAPP $\alpha$  and sAPP $\beta$  specific ELISA (IBL) and Western blot analysis.

#### Transcription-based copper sensor reporter assay

The relative amounts of cytosolic copper were measured with a transcription-based copper sensor reporter assay (32). 25,000 HEK293T cells/well were seeded on poly-D-lysine-coated (Sigma) 24-well plates (Fisher). Cells were transiently transfected 20–24 h later by using TransFectin according to the manufacturer's protocol (Bio-Rad). Per well, 0.2  $\mu\text{g}$  of pGL3-E1b-TATA-4MRE, 0.02  $\mu\text{g}$  of RL-TK, 10 pmol of siRNA (total amount), and where indicated 0.2  $\mu\text{g}$  of BACE1-constructs in pcDNA3.1 (Zeo) were transfected. After 24 or 48 h (for rescue experiments), cells were washed with 1 ml of PBS<sup>2+</sup> and treated with 100  $\mu\text{M}$  CuCl<sub>2</sub>, 1  $\mu\text{M}$  inhibitor IV (in DMSO, Millipore), or 0.01% DMSO in DMEM (high glucose (4.5 g/liter), 10% fetal bovine serum (FBS), 2 mM glutamine, 1 mM pyruvate) for 24 h. Cells were washed again with 1 ml of PBS<sup>2+</sup> and lysed in 100  $\mu\text{l}$  of passive-lysis buffer according to the manufacturer's instructions (Promega). Dual luciferase activity was measured according to manufacturer's instructions (Promega).

#### ICP-MS measurements

1,000,000 HEK293T cells were seeded on poly-D-lysine-coated (Sigma) 10-cm plates (Fisher). For blank measurements, the exact same procedure was performed without cells. Cells were transiently transfected 20–24 h later by using RNAiMax according to the manufacturer's protocol (Invitrogen). Per plate, 82 pmol of siRNA were transfected. After 24 h, cells were treated without or with 100  $\mu\text{M}$  CuCl<sub>2</sub> in DMEM (high glucose (4.5 g/liter), 10% FBS, 2 mM glutamine, 1 mM pyruvate) for 24 h. Cells were washed again three times with 12 ml of PBS<sup>2+</sup> and harvested by scraping in PBS. Cell suspension was separated into two tubes, one for lysis/protein determination, the other for HNO<sub>3</sub> digestion and ICP-MS measurement. Lysates (lysed in PBS, 1% Triton X-100, 2 $\times$  Complete protease inhibitor) were subjected to colorimetric protein determination using a BCA assay (Pierce), according to the manufacturer's protocol. HNO<sub>3</sub> digestion of cell pellets was carried out in trace-analysis grade nitric acid (Sigma) at 95  $^{\circ}\text{C}$  for 1 h. ICP-MS analysis was performed at the Centre for Biological Applications of Mass Spectrometry at Concordia University, using an Agilent 7500 series ICP-MS instrument.

#### Statistical analysis

The statistical evaluation was carried out by GraphPad Prism, SPSS, and the indicated statistical tests and algorithms.

**Author contributions**—F. L. designed and performed experiments, analyzed data, prepared the figures, and wrote the manuscript; H. M., M. R. P. A., T. B., and S. S. designed and performed experiments, analyzed data, and helped write the manuscript. A. H., D. B., and R. B. designed experiments, analyzed data, and helped to write the manuscript. G. M. conceived the study, designed experiments, analyzed data, and wrote the manuscript. All authors have approved the final version of the manuscript.

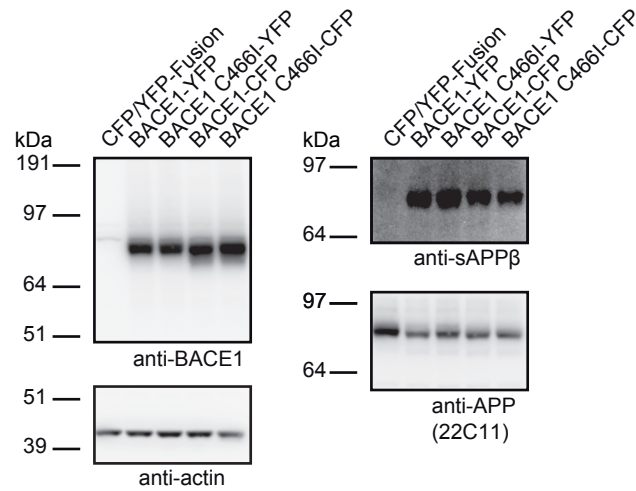
**Acknowledgments**—We thank Drs. Michael Schäfer and Philipp Voigt (University Leipzig) for the pcDNA3-CFP and -YFP constructs, Dr. Leo Klomp (University Medical Center Utrecht) for copper reporter constructs, Dr. Thomas P. Sakmar (Rockefeller University) for constructs to introduce unnatural amino acids, Dr. Alain Tessier (Concordia University) at the Centre for Biological Applications of Mass Spectrometry for performing ICP-MS measurements, Dr. Mark A. Hancock (McGill SPR-MS Facility), and Dr. Patricia M. G. E. Brown (McGill University) for discussions.

#### References

- Luo, Y., Bolon, B., Kahn, S., Bennett, B. D., Babu-Khan, S., Denis, P., Fan, W., Kha, H., Zhang, J., Gong, Y., Martin, L., Louis, J. C., Yan, Q., Richards, W. G., Citron, M., and Vassar, R. (2001) Mice deficient in bace1, the Alzheimer's  $\beta$ -secretase, have normal phenotype and abolished  $\beta$ -amyloid generation. *Nat. Neurosci.* **4**, 231–232
- Vassar, R. (2014) Bace1 inhibitor drugs in clinical trials for Alzheimer's disease. *Alzheimers Res. Ther.* **6**, 89
- Kandalepas, P. C., and Vassar, R. (2012) Identification and biology of  $\beta$ -secretase. *J. Neurochem.* **120**, 55–61
- De Strooper, B., Iwatsubo, T., and Wolfe, M. S. (2012) Presenilins and  $\gamma$ -secretase: structure, function, and role in Alzheimer disease. *Cold Spring Harb. Perspect. Med.* **2**, a006304
- Citron, M., Teplow, D. B., and Selkoe, D. J. (1995) Generation of amyloid  $\beta$  protein from its precursor is sequence specific. *Neuron* **14**, 661–670
- Vetrivel, K. S., Barman, A., Chen, Y., Nguyen, P. D., Wagner, S. L., Prabhakar, R., and Thinakaran, G. (2011) Loss of cleavage at  $\beta$ -site contributes to apparent increase in  $\beta$ -amyloid peptide (A $\beta$ ) secretion by  $\beta$ -secretase (BACE1)-glycosylphosphatidylinositol (GPI) processing of amyloid precursor protein. *J. Biol. Chem.* **286**, 26166–26177
- Zhao, Y., Wang, Y., Hu, J., Zhang, X., and Zhang, Y. W. (2012) CutA divalent cation tolerance homolog (*Escherichia coli*) (CutA) regulates  $\beta$ -cleavage of  $\beta$ -amyloid precursor protein (APP) through interacting with  $\beta$ -site APP cleaving protein 1 (BACE1). *J. Biol. Chem.* **287**, 11141–11150
- Fukumoto, H., Takahashi, H., Tarui, N., Matsui, J., Tomita, T., Hirode, M., Sagayama, M., Maeda, R., Kawamoto, M., Hirai, K., Terauchi, J., Sakura, Y., Kakahana, M., Kato, K., Iwatsubo, T., and Miyamoto, M. (2010) A non-competitive BACE1 inhibitor tak-070 ameliorates A $\beta$  pathology and behavioral deficits in a mouse model of Alzheimer's disease. *J. Neurosci.* **30**, 11157–11166
- Angeletti, B., Waldron, K. J., Freeman, K. B., Bawagan, H., Hussain, I., Miller, C. C., Lau, K. F., Tennant, M. E., Dennison, C., Robinson, N. J., and Dingwall, C. (2005) BACE1 cytoplasmic domain interacts with the copper chaperone for superoxide dismutase-1 and binds copper. *J. Biol. Chem.* **280**, 17930–17937
- Gray, E. H., De Vos, K. J., Dingwall, C., Perkinson, M. S., and Miller, C. C. (2010) Deficiency of the copper chaperone for superoxide dismutase increases amyloid- $\beta$  production. *J. Alzheimers Dis.* **21**, 1101–1105
- Aller, S. G., Eng, E. T., De Feo, C. J., and Unger, V. M. (2004) Eukaryotic copper uptake transporters require two faces of the third transmembrane domain for helix packing, oligomerization, and function. *J. Biol. Chem.* **279**, 53435–53441
- Haas, K. L., Putterman, A. B., White, D. R., Thiele, D. J., and Franz, K. J. (2011) Model peptides provide new insights into the role of histidine residues as potential ligands in human cellular copper acquisition via Ctr1. *J. Am. Chem. Soc.* **133**, 4427–4437
- Lee, J., Peña, M. M., Nose, Y., and Thiele, D. J. (2002) Biochemical characterization of the human copper transporter Ctr1. *J. Biol. Chem.* **277**, 4380–4387
- Munter, L. M., Sieg, H., Bethge, T., Liebsch, F., Bierkandt, F. S., Schleeper, M., Bittner, H. J., Heberle, J., Jakubowski, N., Hildebrand, P. W., and Multhaup, G. (2013) Model peptides uncover the role of the  $\beta$ -secretase transmembrane sequence in metal ion mediated oligomerization. *J. Am. Chem. Soc.* **135**, 19354–19361

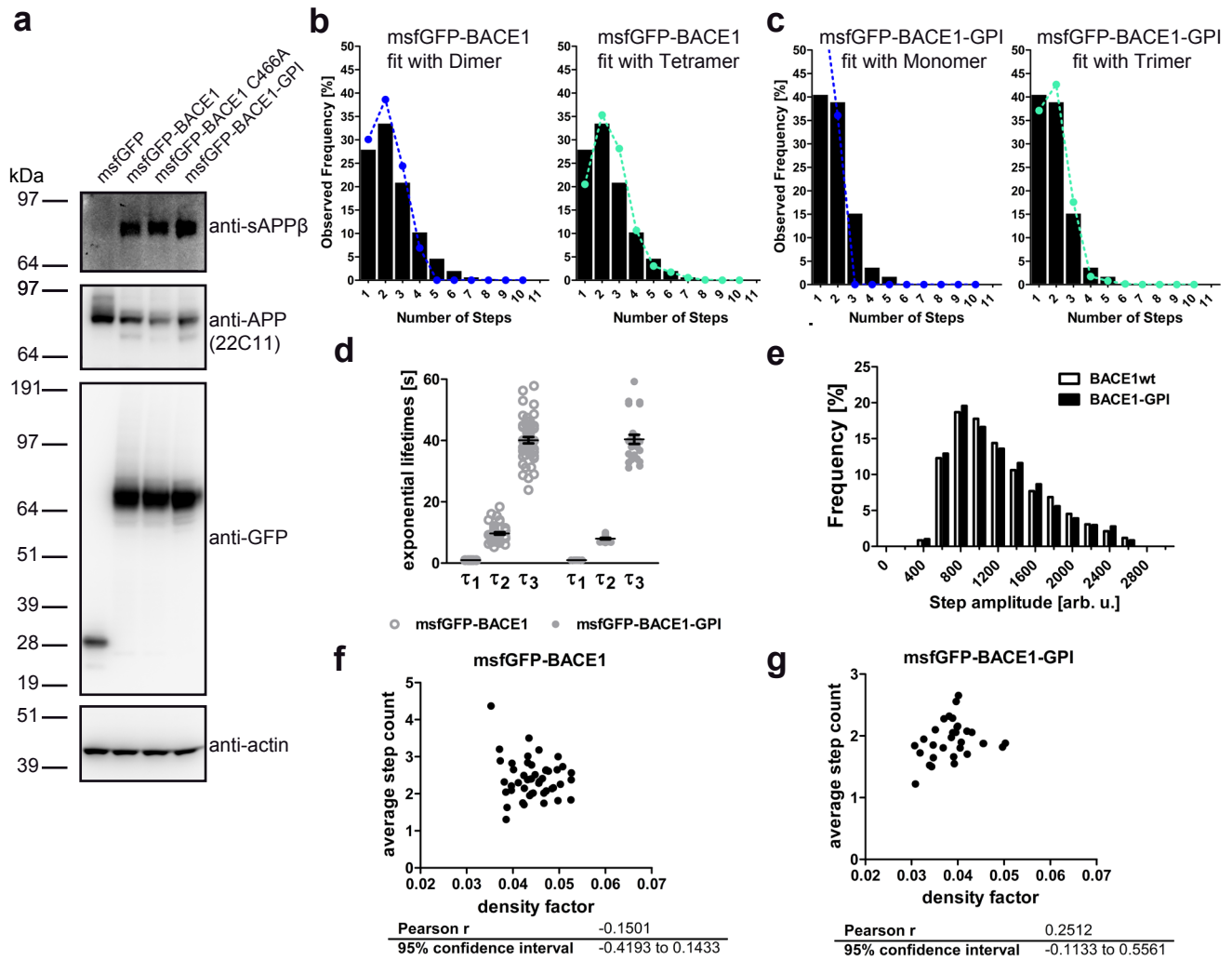
## BACE1 trimerizes and regulates copper homeostasis

- Kuhn, P. H., Koroniak, K., Hogg, S., Colombo, A., Zeitschel, U., Willem, M., Volbracht, C., Schepers, U., Imhof, A., Hoffmeister, A., Haass, C., Roßner, S., Bräse, S., and Lichtenthaler, S. F. (2012) Secretome protein enrichment identifies physiological bace1 protease substrates in neurons. *EMBO J.* **31**, 3157–3168
- Palm-Espling, M. E., Niemiec, M. S., and Wittung-Stafshede, P. (2012) Role of metal in folding and stability of copper proteins *in vitro*. *Biochim. Biophys. Acta* **1823**, 1594–1603
- Lutsenko, S. (2016) Copper trafficking to the secretory pathway. *Metalomics* **8**, 840–852
- Kim, B.-E., Nevitt, T., and Thiele, D. J. (2008) Mechanisms for copper acquisition, distribution and regulation. *Nat. Chem. Biol.* **4**, 176–185
- Menkes, J. H., Alter, M., Steigleder, G. K., Weakley, D. R., and Sung, J. H. (1962) A sex-linked recessive disorder with retardation of growth, peculiar hair, and focal cerebral and cerebellar degeneration. *Pediatrics* **29**, 764–779
- Gitlin, J. D. (2003) Wilson disease. *Gastroenterology* **125**, 1868–1877
- McGuire, H., Arousseau, M. R., Bowie, D., and Blunck, R. (2012) Automating single subunit counting of membrane proteins in mammalian cells. *J. Biol. Chem.* **287**, 35912–35921
- Engel, S., Scolari, S., Thaa, B., Krebs, N., Korte, T., Herrmann, A., and Veit, M. (2010) FLIM-FRET and FRAP reveal association of influenza virus haemagglutinin with membrane rafts. *Biochem. J.* **425**, 567–573
- Ulbrich, M. H., and Isacoff, E. Y. (2007) Subunit counting in membrane-bound proteins. *Nat. Methods* **4**, 319–321
- Westmeyer, G. G., Willem, M., Lichtenthaler, S. F., Lurman, G., Multhaup, G., Assfalg-Machleidt, I., Reiss, K., Saftig, P., and Haass, C. (2004) Dimerization of  $\beta$ -site  $\beta$ -amyloid precursor protein-cleaving enzyme. *J. Biol. Chem.* **279**, 53205–53212
- Cordy, J. M., Hussain, I., Dingwall, C., Hooper, N. M., and Turner, A. J. (2003) Exclusively targeting  $\beta$ -secretase to lipid rafts by GPI-anchor addition up-regulates  $\beta$ -site processing of the amyloid precursor protein. *Proc. Natl. Acad. Sci. U.S.A.* **100**, 11735–11740
- Nie, L., Lavinder, J. J., Sarkar, M., Stephany, K., and Magliery, T. J. (2011) Synthetic approach to stop-codon scanning mutagenesis. *J. Am. Chem. Soc.* **133**, 6177–6186
- Soskine, M., Steiner-Mordoch, S., and Schuldiner, S. (2002) Crosslinking of membrane-embedded cysteines reveals contact points in the emre oligomer. *Proc. Natl. Acad. Sci. U.S.A.* **99**, 12043–12048
- Johnston, J. M., Aburi, M., Provasi, D., Bortolato, A., Urizar, E., Lambert, N. A., Javitch, J. A., and Filizola, M. (2011) Making structural sense of dimerization interfaces of  $\delta$  opioid receptor homodimers. *Biochemistry* **50**, 1682–1690
- Bagchi, P., Morgan, M. T., Bacsá, J., and Fahrni, C. J. (2013) Robust affinity standards for Cu(I) biochemistry. *J. Am. Chem. Soc.* **135**, 18549–18559
- Borchardt, T., Camakaris, J., Cappai, R., Masters, C. L., Beyreuther, K., and Multhaup, G. (1999) Copper inhibits  $\beta$ -amyloid production and stimulates the non-amyloidogenic pathway of amyloid-precursor-protein secretion. *Biochem. J.* **344**, 461–467
- Huse, J. T., Pijak, D. S., Leslie, G. J., Lee, V. M., and Doms, R. W. (2000) Maturation and endosomal targeting of  $\beta$ -site amyloid precursor protein-cleaving enzyme: the Alzheimer's disease  $\beta$ -secretase. *J. Biol. Chem.* **275**, 33729–33737
- van den Berghe, P. V., Folmer, D. E., Malingré, H. E., van Beurden, E., Klomp, A. E., van de Sluis, B., Merckx, M., Berger, R., and Klomp, L. W. (2007) Human copper transporter 2 is localized in late endosomes and lysosomes and facilitates cellular copper uptake. *Biochem. J.* **407**, 49–59
- Polishchuk, E. V., Concilli, M., Iacobacci, S., Chesi, G., Pastore, N., Piccolo, P., Paladino, S., Baldantoni, D., van IJzendoorn, S. C., Chan, J., Chang, C. J., Amoresano, A., Pane, F., Pucci, P., Tarallo, A., *et al.* (2014) Wilson disease protein Atp7b utilizes lysosomal exocytosis to maintain copper homeostasis. *Dev. Cell* **29**, 686–700
- Barnes, N., Bartee, M. Y., Braiterman, L., Gupta, A., Ustiyán, V., Zuzel, V., Kaplan, J. H., Hubbard, A. L., and Lutsenko, S. (2009) Cell-specific trafficking suggests a new role for renal Atp7b in the intracellular copper storage. *Traffic* **10**, 767–779
- Stachel, S. J., Coburn, C. A., Steele, T. G., Jones, K. G., Loutzenhiser, E. F., Gregro, A. R., Rajapakse, H. A., Lai, M.-T., Crouthamel, M.-C., Xu, M., Tugusheva, K., Lineberger, J. E., Pietrak, B. L., Espeseth, A. S., Shi, X.-P., *et al.* (2004) Structure-based design of potent and selective cell-permeable inhibitors of human  $\beta$ -secretase (BACE-1). *J. Med. Chem.* **47**, 6447–6450
- Vita, N., Platsaki, S., Baslé, A., Allen, S. J., Paterson, N. G., Crombie, A. T., Murrell, J. C., Waldron, K. J., and Dennison, C. (2015) A four-helix bundle stores copper for methane oxidation. *Nature* **525**, 140–143
- Wu, J., Forbes, J. R., Chen, H. S., and Cox, D. W. (1994) The lec rat has a deletion in the copper transporting ATPase gene homologous to the Wilson disease gene. *Nat. Genet.* **7**, 541–545
- Lutsenko, S. (2008) Atp7b<sup>-/-</sup> mice as a model for studies of Wilson's disease. *Biochem. Soc. Trans.* **36**, 1233–1238
- Meyer, L. A., Durlay, A. P., Prohaska, J. R., and Harris, Z. L. (2001) Copper transport and metabolism are normal in aceruloplasminemic mice. *J. Biol. Chem.* **276**, 36857–36861
- Banci, L., Bertini, I., Cantini, F., and Ciofi-Baffoni, S. (2010) Cellular copper distribution: a mechanistic systems biology approach. *Cell. Mol. Life Sci.* **67**, 2563–2589
- Banci, L., Bertini, I., Ciofi-Baffoni, S., Kozyreva, T., Zovo, K., and Palumaa, P. (2010) Affinity gradients drive copper to cellular destinations. *Nature* **465**, 645–648
- Schmechel, A., Strauss, M., Schlicksupp, A., Pipkorn, R., Haass, C., Bayer, T. A., and Multhaup, G. (2004) Human BACE forms dimers and colocalizes with APP. *J. Biol. Chem.* **279**, 39710–39717
- Ye, S., Huber, T., Vogel, R., and Sakmar, T. P. (2009) FTIR analysis of GPCR activation using azido probes. *Nat. Chem. Biol.* **5**, 397–399
- Ye, S., Köhrer, C., Huber, T., Kazmi, M., Sachdev, P., Yan, E. C., Bhagat, A., Rajbhandary, U. L., and Sakmar, T. P. (2008) Site-specific incorporation of keto amino acids into functional G protein-coupled receptors using unnatural amino acid mutagenesis. *J. Biol. Chem.* **283**, 1525–1533
- Munter, L.-M., Voigt, P., Harmeier, A., Kaden, D., Gottschalk, K. E., Weise, C., Pipkorn, R., Schaefer, M., Langosch, D., and Multhaup, G. (2007) GxxxG motifs within the amyloid precursor protein transmembrane sequence are critical for the etiology of  $\alpha\beta$ 42. *EMBO J.* **26**, 1702–1712
- Kaden, D., Harmeier, A., Weise, C., Munter, L. M., Althoff, V., Rost, B. R., Hildebrand, P. W., Schmitz, D., Schaefer, M., Lurz, R., Skodda, S., Yamamoto, R., Arlt, S., Finckh, U., and Multhaup, G. (2012) Novel APP/A $\alpha\beta$  mutation K16N produces highly toxic heteromeric A $\beta$  oligomers. *EMBO Mol. Med.* **4**, 647–659
- Voigt, P., Brock, C., Nürnberg, B., and Schaefer, M. (2005) Assigning functional domains within the p101 regulatory subunit of phosphoinositide 3-kinase  $\gamma$ . *J. Biol. Chem.* **280**, 5121–5127
- Lackowicz, J. (ed) (2006) *Principles of Fluorescence Spectroscopy, 3rd Ed.*, Springer Science & Business Media, New York
- Scolari, S., Engel, S., Krebs, N., Plazzo, A. P., De Almeida, R. F., Prieto, M., Veit, M., and Herrmann, A. (2009) Lateral distribution of the transmembrane domain of influenza virus hemagglutinin revealed by time-resolved fluorescence imaging. *J. Biol. Chem.* **284**, 15708–15716



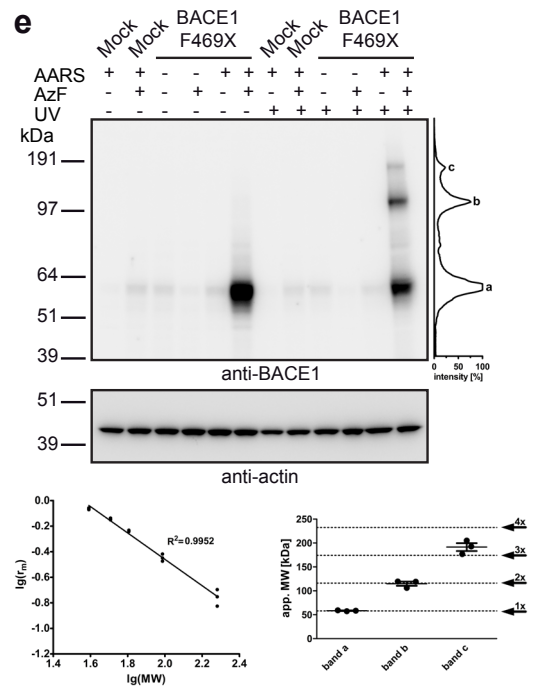
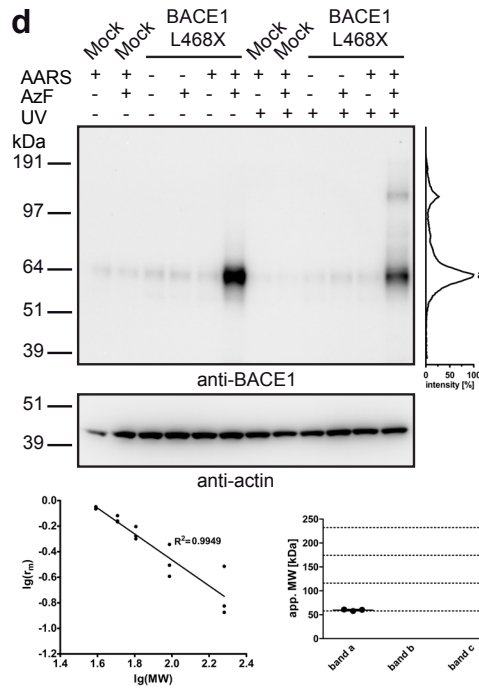
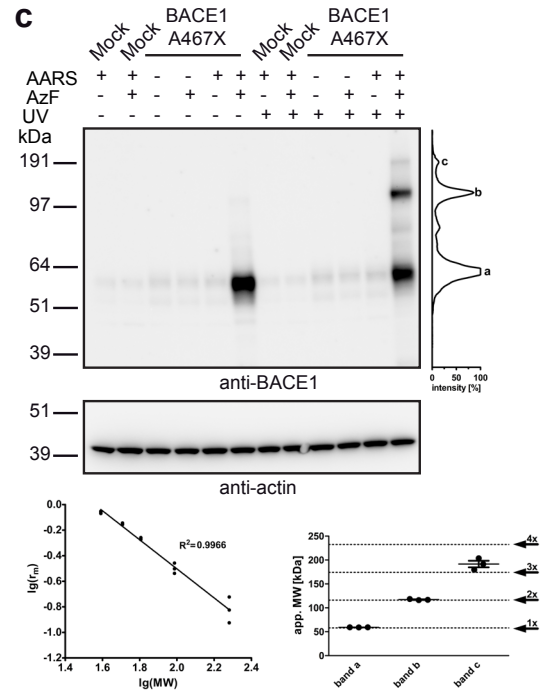
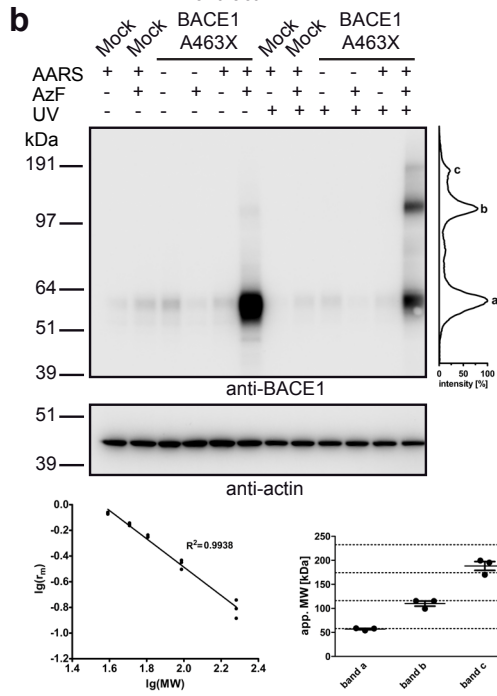
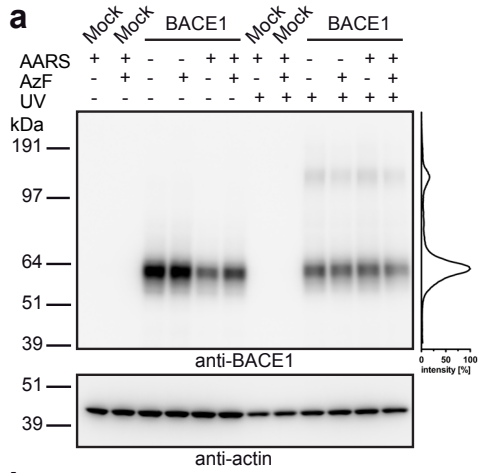
**Supplementary Figure 1: FLIM-FRET constructs expression/activity control.**

APP cleavage by fluorophore-tagged BACE1 was analyzed by co-transfection of APP695wt and BACE1 constructs. sAPP $\beta$  was detected by Western blot analysis from conditioned medium after 8 h. Cells were lysed and APP and BACE1 expression was analyzed by Western blot, APP (22C11), BACE1-CFP/-YFP (EE-17). Representative blots are shown; experiments were replicated 3 times.



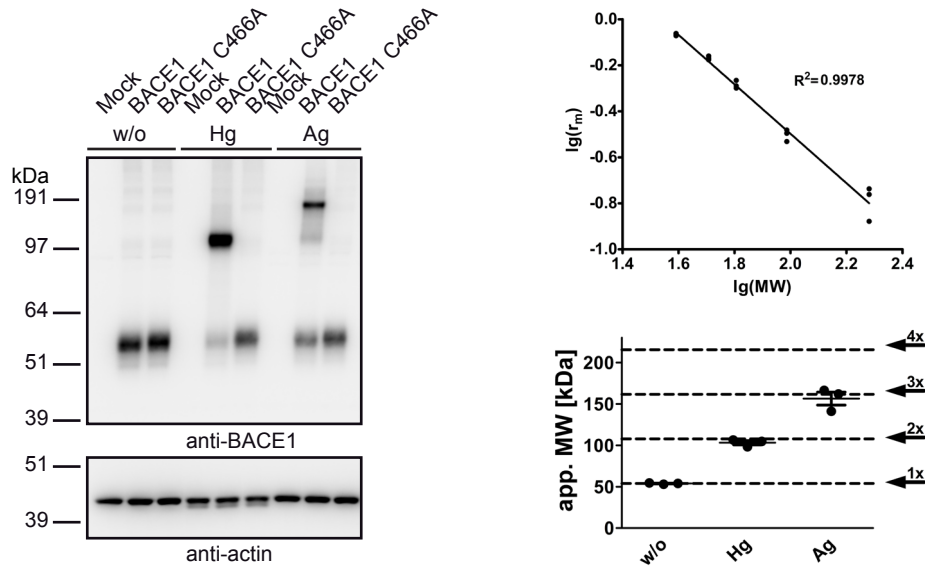
### Supplementary Figure 2: Single-molecule fluorescence counting.

(a) APP cleavage by fluorophore-tagged BACE1 was analyzed by co-transfection of APP695wt and BACE1 constructs. APP (22C11), msfGFP-BACE1 (anti-GFP) from lysates, and sAPP $\beta$  from conditioned medium after 8 h were detected by Western blot analysis. Representative blots are shown; experiments were replicated 3 times. (b-g) Data were obtained from 2086 traces, 47 cells, 4 transfections for BACE1 wt and 1139 traces, 29 cells, 3 transfections for BACE1-GPI. (b,c) Histogram of observed step frequency distribution was fit with a fixed probability of fluorescence ( $p_m$ ),  $p_m=0.53$ . (b) The data for msf-GFP-BACE1 were not well fit (as indicated by the high  $SE^2$ ) for dimers ( $SE^2=80.63$ ) and tetramers ( $SE^2=113.79$ ) (s. Figure 2b). (c) The data for msf-GFP-BACE1-GPI were not well fit for monomers ( $SE^2=790.03$ ) and trimers ( $SE^2=42.38$ ) (s. Figure 2c). (d) The exponential time constants  $\sigma_1$ ,  $\sigma_2$ ,  $\sigma_3$ , for BACE1 and BACE1-GPI. Horizontal lines indicate means  $\pm$  s.e.m. The data were analyzed with a between-subject 2-way ANOVA, interaction  $F(2,210) = 0.93$ ,  $p = 0.398$ . (e) Histogram of step amplitude distributions for BACE1 and BACE1-GPI. (f,g) Plots of the average step count against the density factor per cell for BACE1 (f) and BACE1-GPI (g). There was no significant correlation between these two parameters ( $p > 0.05$ ) and the step count was independent of the expression level.



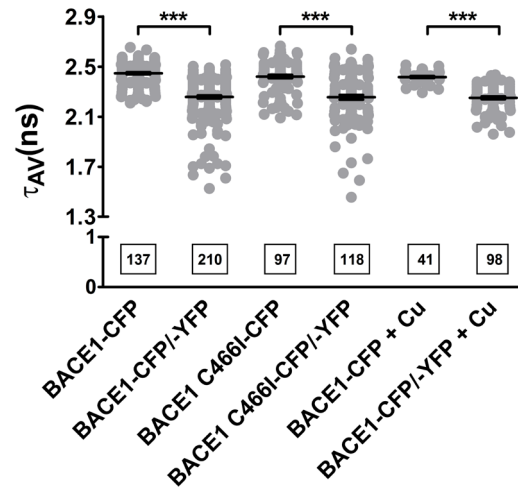
**Supplementary Figure 3: Western blot Analysis of BACE1 with and without pAzF incorporated at indicated positions.**

(a-e) Cells were transfected with empty vector (Mock) or BACE1 with or without Amber-Stop codon at the indicated positions (463, 466, 467, 468, and 469) and co-transfected with aminoacyl-tRNA-synthetase Tyr-RS-pAzF (AARS). The multimeric state of BACE1 was analyzed using Western blot analysis under reducing and denaturing conditions. Faint, non-specific dimer bands were generated by UV-treatment of BACE1-expressing cells. Densitometry profiles of the relative abundance of cross-linked multimeric BACE1 species were analyzed using ImageJ software and are shown adjacent to the gel lanes; actin was used as control. Representative blots are shown for BACE1 (a), BACE1-A463X (b), BACE1-A467X (c), BACE1-L468X (d), and BACE1-F469X (e). Independent experiments were replicated 3 times. (b-e) The decadic logarithm of the relative mobility ( $r_m$ ) of the protein standards plotted against the decadic logarithm of the apparent molecular weight (MW) between 39 and 191 kDa. The calculation of apparent MW of monomeric (1x) BACE1 yielded 58.10 kDa. The apparent MW of bands b and c correspond to the theoretical apparent MW of dimers and trimers (dashed lines). Horizontal lines indicate the mean apparent MW  $\pm$  s.e.m.



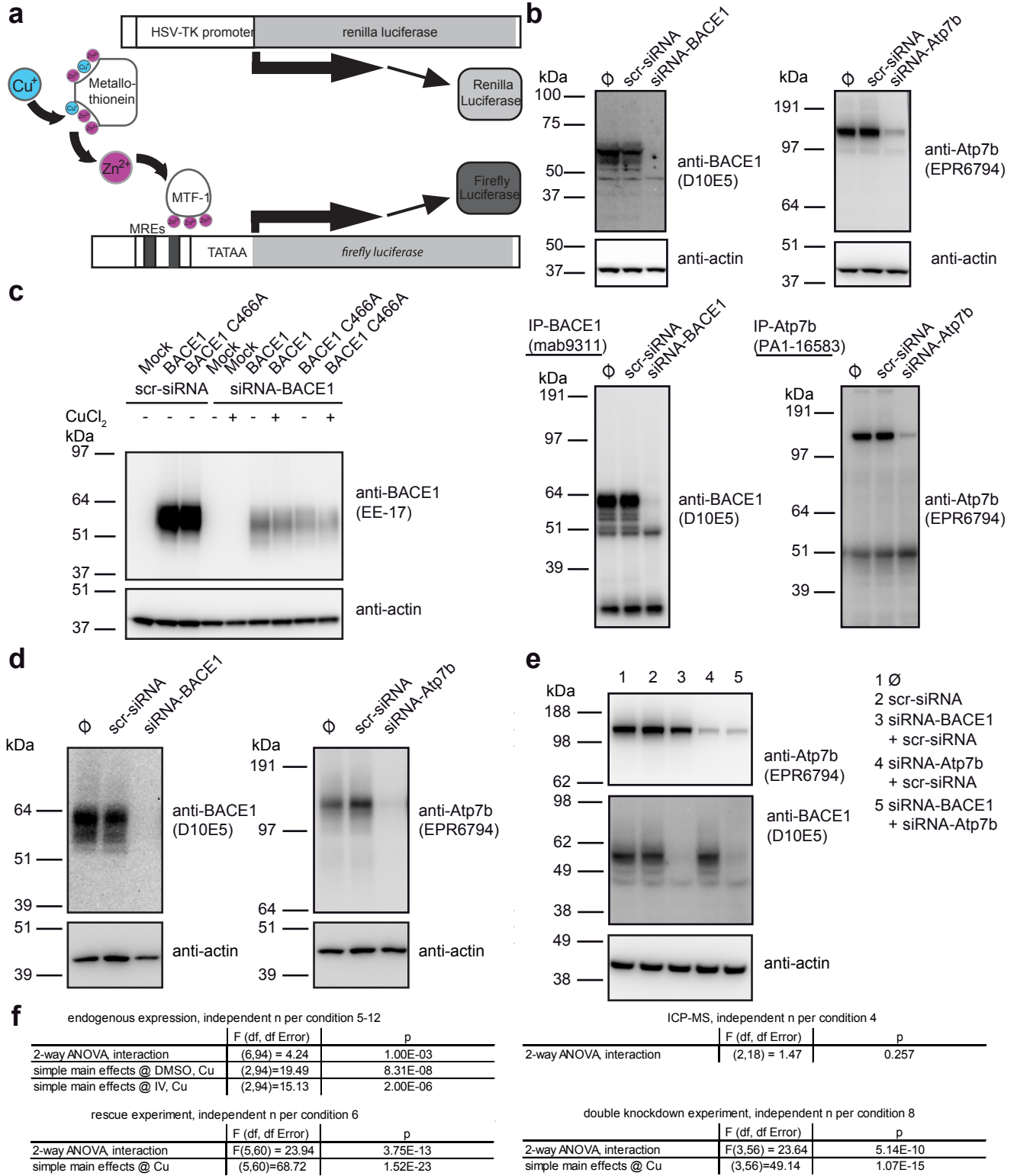
**Supplementary Figure 4: Western blot Analysis of Cys466 chemically cross-linked BACE1.**

Cells were transfected with empty vector (Mock), BACE1, or BACE1 C466A and treated with  $\text{HgCl}_2$  or  $\text{AgNO}_3$ . The multimeric state was analyzed using Western blot analysis under non-reducing conditions. Representative blots of three independently replicated experiments are shown. The decadic logarithm of the relative mobility ( $r_m$ ) of the protein standards plotted against the decadic logarithm of the apparent molecular weight (MW) between 39 and 191 kDa. The calculation of apparent MW of monomeric (1x) BACE1 yielded 53.88 kDa. The apparent MW of BACE1 in the presence of Hg and Ag correspond to the theoretical apparent MW of dimers and trimers (dashed lines). Horizontal lines indicate the mean apparent MW  $\pm$  s.e.m.



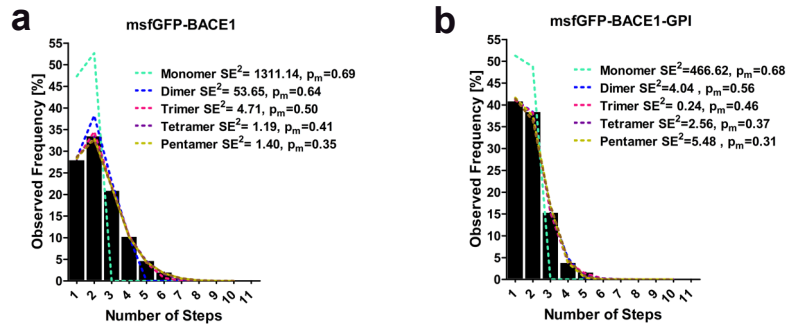
**Supplementary Figure 5: FLIM-FRET measurements.**

Fluorescence lifetime of CFP was measured in the plasma membrane of transiently transfected HEK293T cells. Columns depict the average lifetimes over all measured cells  $\pm$  s.e.m. (on average 10 cells per dish were measured; the total number of measured cells is given at the bottom of each column). BACE1-CFP and -YFP are shown again for better comparison (same data as in Figure 1d). Where indicated cells were treated with 100  $\mu$ M  $\text{CuCl}_2$ . The data were analyzed with a 1-WAY ANOVA,  $F(7,848)=34.83$ , \*\*\*  $p < 0.0001$ ; Tukey's post-hoc test, selected comparisons are highlighted, \*\*\*  $p < 0.0001$ ).



**Supplementary Figure 6: Western blot Analysis of BACE1 and Atp7b knockdown.**

(a) Luciferase reporter gene assay was used to detect changes in intracellular copper levels. Gene expression was measured by dual-luciferase assay; metal-regulatory transcription factor 1 (MTF-1), metal-responsive elements (MRE), herpes simplex virus (HSV), thymidine kinase (TK). (b) Western blot analysis of endogenous BACE1 (left) and Atp7b (right) from HEK293T cell lysates (top) or immunoprecipitated (bottom), 48 h after co-transfection with MRE-firefly-luciferase, HSV-TK-renilla-luciferase, and either no siRNA ( $\emptyset$ ), scrambled siRNA (scr-siRNA), BACE1-specific siRNA (siRNA-BACE1), or Atp7b-specific siRNA (siRNA-Atp7b). Representative blots of 3 independent experiments. (c) Western blot analysis of knockdown-resistant BACE1 and BACE1 C466A expression in the background of scr-siRNA or siRNA-BACE1, 72 h after co-transfection with MRE- firefly-luciferase and HSV-TK-renilla-luciferase. The experiments were independently replicated 4 times. (d) Western blot analysis of endogenous BACE1 (left) and Atp7b (right) from HEK293T cells for ICP-MS analysis, 48 h after transfection with  $\emptyset$ , scr-siRNA, siRNA-BACE1, siRNA-Atp7b. Representative blots from 3 independent experiments. (e) ) Western blot analysis of endogenous BACE1 (bottom) and Atp7b (top) from HEK293T cells, 48 h after transfection with  $\emptyset$ , scr-siRNA, siRNA-BACE1 + scr-siRNA, siRNA-Atp7b + scr-siRNA, siRNA-BACE1 + siRNA-Atp7b. Representative blots from 3 independent experiments. (f) Results from statistical analyses of indicated experiments.



**Supplementary Figure 7: Single-molecule fluorescence counting.**

Data were obtained from 2086 traces, 47 cells, 4 transfections for BACE1 and 1139 traces, 29 cells, 3 transfections for BACE1-GPI. (a,b) Histogram of observed step frequency distribution for BACE1 (a) and for BACE1-GPI (b) were fit with free-floating  $p_m$ .

**Full-length cellular  $\beta$ -secretase has a trimeric subunit stoichiometry, and its sulfur-rich transmembrane interaction site modulates cytosolic copper compartmentalization**

Filip Liebsch, Mark R. P. Arousseau, Tobias Bethge, Hugo McGuire, Silvia Scolari, Andreas Herrmann, Rikard Blunck, Derek Bowie and Gerd Multhaup

*J. Biol. Chem.* 2017, 292:13258-13270.

doi: 10.1074/jbc.M117.779165 originally published online June 21, 2017

---

Access the most updated version of this article at doi: [10.1074/jbc.M117.779165](https://doi.org/10.1074/jbc.M117.779165)

Alerts:

- [When this article is cited](#)
- [When a correction for this article is posted](#)

[Click here](#) to choose from all of JBC's e-mail alerts

Supplemental material:

<http://www.jbc.org/content/suppl/2017/06/21/M117.779165.DC1>

This article cites 48 references, 25 of which can be accessed free at <http://www.jbc.org/content/292/32/13258.full.html#ref-list-1>